

THE DEFORMATION BEHAVIOUR OF FIBRE-REINFORCED COPPER

by

GRAEME CLAUDE HOWARD

A THESIS SUBMITTED IN PARTIAL FULFILMENT  
OF THE REQUIREMENTS FOR THE DEGREE OF  
MASTER OF APPLIED SCIENCE  
IN THE DEPARTMENT  
OF  
METALLURGY

We accept this thesis as conforming to the  
standard required from candidates for  
the degree of  
MASTER OF APPLIED SCIENCE

Members of the Department of Metallurgy

THE UNIVERSITY OF BRITISH COLUMBIA

March, 1964

In presenting this thesis in partial fulfilment of the requirements for an advanced degree at the University of British Columbia, I agree that the Library shall make it freely available for reference and study. I further agree that permission for extensive copying of this thesis for scholarly purposes may be granted by the Head of my Department or by his representatives. It is understood that copying or publication of this thesis for financial gain shall not be allowed without my written permission.

Department of Metallurgy

The University of British Columbia,  
Vancouver 8, Canada.

Date March 1964

## ABSTRACT

The deformation behaviour of copper, reinforced with iron and steel fibres has been investigated. Parameters studied include: fibre diameter, matrix mean free path, and relative strength of fibre and matrix.

No strengthening effect has been observed which can be attributed to fibre size alone. However, it is suggested that the strength of metal fibre-reinforced metal composites are greatly influenced by a "size effect" in the matrix.

A modification of the theory of combined action has been proposed for predicting the strength of a fibre-reinforced composite, viz:

$$\sigma_c = A_f \sigma_f + A_m \sigma_m + A_f^{1/4} K d_f^{-1/2}$$

where A is volume fraction, f refers to fibre, m refers to matrix,  $d_f$  is fibre diameter, and K is a constant whose value depends on the hardness of the fibre.

Weakening of the matrix-fibre interface in composites of copper and steel fibres has been attributed to segregation of carbon to the interface.

Alloys containing 6 to 8 weight per cent copper in iron have been shown to exhibit a martensitic transformation when cooled from the  $\gamma$  region of the Fe-Cu phase diagram.

## TABLE OF CONTENTS

	Page
I. INTRODUCTION . . . . .	1
A. General . . . . .	1
B. Previous Work . . . . .	2
C. Scope . . . . .	9
II. EXPERIMENTAL PROCEDURE . . . . .	11
A. Materials . . . . .	11
B. Composite Preparation . . . . .	12
1. Wire Composites . . . . .	12
2. Powder Composites . . . . .	13
C. Swaging and Drawing . . . . .	16
D. Heat Treating . . . . .	16
E. Measurement of Fibre Concentration . . . . .	18
F. Tensile Testing . . . . .	18
G. Metallography . . . . .	18
III. RESULTS . . . . .	19
A. Composites Made From High Carbon Steel Wire Bundles . . . . .	19
1. Structures . . . . .	19
2. Size Effects . . . . .	22
3. Studies of Heterogeneous Yielding . . . . .	29
a) Effect of Cold Working . . . . .	32
b) Properties of Single Steel Wires . . . . .	32
c) Effect of Interrupted Loading . . . . .	32
d) Effect of Strain Ageing . . . . .	32
e) Observations During Loading . . . . .	35
B. Composites Made From Sintered Armco Iron Powder . . . . .	35
1. Structures . . . . .	35
2. Size Effects . . . . .	37
3. Heterogeneous Yielding . . . . .	43
4. Heat Treatments on Saturated Iron Powder Composites . . . . .	44
a) Results with -100 +150 mesh Powder Composites . . . . .	44
b) Results with -325 mesh Powder Composites . . . . .	48
IV. DISCUSSION . . . . .	57
A. Structure and Aspect Ratios of Composites . . . . .	57
B. Yield Behaviour of Unsaturated Powder Composites . . . . .	59
1. Heterogeneous Yielding . . . . .	59
2. Size Dependence of Yield Stress . . . . .	60
C. Yield Behaviour of Wire Composites . . . . .	61
1. Origin of Two Yield Points . . . . .	61
2. Heterogeneous Yielding . . . . .	61
3. Size Dependence of Yield Stress . . . . .	64
D. Effect of Heat Treatment on Saturated Powder Composites . . . . .	65
E. Deformation Behaviour of Metal Fibre Reinforced Metals . . . . .	73

## Table of Contents Continued..

	Page
V. CONCLUSIONS . . . . .	79
VI. SUGGESTED FUTURE WORK . . . . .	80
VII. BIBLIOGRAPHY . . . . .	81
VIII. APPENDICES . . . . .	83

## LIST OF FIGURES

Figure	Page
1. Schematic Relation Between Fibre Tensile Stress ( $\sigma_f$ ) Interfacial Shear Stress ( $\tau$ ) and Fibre Length . . .	5
2. Relationship Between Composite Tensile Strength and Volume Per Cent Fibres for Various Fibre Lengths . . .	6
3. Tensile Strengths of Wires Drawn from Several Alloys, Reproduced from Roberts <sup>16</sup> . . . . .	9
4. System for Infiltration of Steel Wire Bundles . . . . .	14
5. Cross-section (a) and Longitudinal Section (b) of Specimen W-1-A-6 . . . . .	20
6. Effect of Annealing 1 hour at 680°C, Specimen W-1-A-11 . . .	21
7. Distribution of Fibres in the Copper Matrix, Specimen W-1-12 . . . . .	21
8. Typical Stress-Plastic Strain Curves for Various Specimen Sizes (a) Composite W-1-A . . . . . (b) Composite W-3-A . . . . .	23 24
9. Composite Yield Stress Versus Specimen Diameter for Composites W-1-A, W-2-A, and W-3-A . . . . .	25
10. Composite Ultimate Tensile Stress Versus Specimen Diameter for Composites W-1-A, W-2-A, and W-3-A . . .	26
11. Method of Determining $Y_{P_{matrix}}$ and $Y_{P_{composite}}$ from Load-Elongation Curves . . . . .	27
12. Matrix Yield Stress Versus Specimen Diameter for Composites W-1-A, W-2-A, and W-3-A . . . . .	28
13. Distance "D" (Figure 11) in Per Cent Elongation Versus Specimen Diameter for Composites W-1-A, W-2-A, and W-3-A . . . . .	30
14. Discontinuous Yield Elongation as Measured From $Y_{P_{composite}}$ Versus Specimen Diameter for Composites W-1-A, W-2-A, and W-3-A . . . . .	31
15. Stress-Plastic Strain Curve For Single Steel Wire . . . . .	34
16. Deformation Bands on Polished Surface of Specimen W4L . . .	36
17. Sections Through Iron Powder Composites . . . . .	38
18. Stress Versus Plastic Strain for Selected Specimen Sizes for -100 +150 mesh Powder Composites . . . . .	39,40

## List of Figures Continued..

Figure	Page
19. Ultimate Tensile Stress Versus Specimen Diameter for -100 +150 mesh Powder Composites . . . . .	41
20. Composite Yield Stress Versus Specimen Diameter for -100 +150 mesh Powder Composites . . . . .	42
21. Photomicrograph of -100 +150 mesh Powder Composite "Aircooled" from 1020°C . . . . .	45
22. Stress-Plastic Strain Curves for Various Heat Treatments on -100 +150 mesh Powder Composites . . . . .	49
23. Photomicrograph of -325 mesh Powder Composite, Quenched in liquid nitrogen and aged for 1 hour at -80°C . . . . .	50
24. Photomicrograph of -325 mesh Powder Composite, Pack carburized at 920°C for 100 minutes . . . . .	54
25. Stress-Plastic Strain Curves for Various Heat Treatments on -325 mesh Powder Composites . . . . .	55
26. Yield Stress Versus Cooling Rate for "Saturated" Iron Powder Composites . . . . .	56
27. Specimen Diameter Versus Predicted Strengths of the Matrix and Fibres . . . . .	66
28. Proposed Cooling-Transformation Diagram for Iron-7% Copper Alloy . . . . .	71
29. Assumed Fibre Distribution . . . . .	75

## LIST OF TABLES

Table	Page
I. Swaging and Drawing Schedule . . . . .	16
II. Work-Hardening Exponents . . . . .	32
III. Strain Ageing Results . . . . .	35
IV. Work-Hardening Exponents . . . . .	43

## ACKNOWLEDGEMENT

The author is grateful for the advice and encouragement given by his research director, Dr. J. A. Lund. Thanks are also extended to other faculty members and fellow graduate students for many helpful discussions.

Financial assistance in the form of Defence Research Board Grants No. 7501-02 and No. 7501-03 is gratefully acknowledged.

## I. INTRODUCTION

### A. General

The advance of science and technology depends to a large degree upon the development of improved structural components. To this end a large amount of time and effort has been allotted to the creation and investigation of composite materials which exploit the best properties of different individual materials.

The greatest strengths in composite materials are found in those which contain a large volume fraction of a dispersed hard phase coupled with a high density of dislocations in the matrix. This type of microstructure can be produced in several ways, including: precipitation at low temperatures from a supersaturated solid solution, eutectoid decomposition, mechanical mixing and subsequent sintering of powders, and internal oxidation of suitable alloys.

A study of the strengthening mechanisms involved in these types of microstructures has led to the realization that the greatest strengths would be achieved if the dispersed hard phase particles were very strong and loaded to fracture. Consequently, considerations have been given to methods of load transfer from the ductile matrix to the harder dispersed phase. The result of such investigations has been the conclusion that greater strengths would be realized if the dispersed particles were needle shaped, thus accommodating maximum load transfer.

Accordingly, recent investigators have considered combining fibrous materials with relatively weak binder materials, thus utilizing the fact that fibres or wires can be exceedingly strong and can exhibit

mechanical properties superior to those of the bulk material from which they are derived. Several techniques have been developed for incorporating strong fibres in relatively weaker matrices and a theory predicting composite strengths has been developed.

#### B. Previous Work

Much of the research associated with the fundamentals of fibre reinforcement has been in the field of glass reinforced plastics. Coleman<sup>1</sup> has statistically related the strength of bundles of fibres to the strength of individual fibres. Coleman's idealized mathematical analysis indicated that the average tensile strength of the bundle would be less than the average strength obtained for the individual fibres making up the bundle.

Paratt<sup>2</sup> has studied the effects of defects in glass fibres and variations in length to diameter ratios (aspect ratios) for both full length and discontinuous fibres.

A method of predicting composite strength termed "The Theory of Combined Action" has been developed by Dietz<sup>3</sup> from his work on fibreglass reinforced plastics. Various workers<sup>4,5,6,7</sup> have shown that this theory is also applicable to metallic and ceramic fibres in metallic matrices. What follows in the present review is a brief discussion of the theory for predicting composite strengths plus an outline of some experimental results pertaining to metallic systems.

For a volume fraction of fibres greater than a certain critical value (to be discussed later) the breaking stress of a fibre composite,

$\sigma_c$ , is given by:

$$\sigma_c = \sigma_f A_f + \sigma'_m A_m \quad \dots\dots(1)$$

where  $\sigma_f$  = the fracture stress of fibres removed from the composite  
 $\sigma'_m$  = the stress supported by the matrix when the fibres fracture  
 $A_f, A_m$  = the volume fractions of the fibres and matrix respectively.

McDanel et al.<sup>8</sup> have generalized equation (1) to allow for the prediction of the stress in a composite at any value of strain, i.e.

$$\sigma_c^* = \sigma_f^* A_f + \sigma_m^* A_m \quad \dots\dots(2)$$

where the  $\sigma^*$ 's represent stresses at a particular value of strain taken from the stress-strain curves of the individual components of the composite, in the condition in which they exist in the composite. McDanel et al. in their work on tungsten-fibre-reinforced copper composites defined four stages of tensile behaviour and applied equation (2) to each one of them. The four stages were:

- I. Elastic deformation of fibre; elastic deformation of matrix,
- II. Elastic deformation of fibre; plastic deformation of matrix,
- III. Plastic deformation of fibre; plastic deformation of matrix,
- IV. Failure of the composite.

Returning to equation (1), it is necessary to consider the effects of low volume fractions of fibres. If the volume per cent of fibres is small, then failure of the fibres need not lead to immediate failure of the composite since the matrix may work-harden sufficiently. Expressing this mathematically, equation (1) holds only if the breaking stress of the composite is greater than that of the matrix, i.e.

$$\sigma_c = \sigma_f A_f + \sigma_m A_m \quad \dots(1)$$

where  $\sigma_f$  = the fracture stress of fibres removed from the composite  
 $\sigma_m$  = the stress supported by the matrix when the fibres fracture  
 $A_f, A_m$  = the volume fractions of the fibres and matrix respectively.

McDanel et al.<sup>8</sup> have generalized equation (1) to allow for the prediction of the stress in a composite at any value of strain, i.e.

$$\sigma_c^{\epsilon} = \sigma_f^{\epsilon} A_f + \sigma_m^{\epsilon} A_m \quad \dots(2)$$

where the  $\sigma^{\epsilon}$ 's represent stresses at a particular value of strain taken from the stress-strain curves of the individual components of the composite, in the condition in which they exist in the composite. McDanel et al. in their work on tungsten-fibre-reinforced copper composites defined four stages of tensile behaviour and applied equation (2) to each one of them. The four stages were:

- I. Elastic deformation of fibre; elastic deformation of matrix,
- II. Elastic deformation of fibre; plastic deformation of matrix,
- III. Plastic deformation of fibre; plastic deformation of matrix,
- IV. Failure of the composite.

Returning to equation (1), it is necessary to consider the effects of low volume fractions of fibres. If the volume per cent of fibres is small, then failure of the fibres need not lead to immediate failure of the composite since the matrix may work-harden sufficiently. Expressing this mathematically, equation (1) holds only if the breaking stress of the composite is greater than that of the matrix, i.e.

$$\sigma_c > \sigma_u A_m \dots\dots(3)$$

where  $\sigma_u$  is the ultimate tensile strength of the matrix.

Combining equations (1) and (3)<sup>6</sup> gives rise to an expression for the critical volume per cent of fibres.

$$A_{fc} = \frac{1}{1 + \frac{\sigma_f}{(\sigma_u - \sigma'_m)}} \dots\dots(4)$$

Dow<sup>9</sup> has done a detailed study of the relationships between the applied load, interfacial shear stresses, and fibre tensile stresses in a filament-reinforced composite metal. A schematic representation of these quantities is shown in Figure 1. Assuming uniform packing and alignment of the fibres and equal straining in the fibres and matrix at their interface, a plausible distribution of shear and tensile stresses is as shown in Figure 1b<sup>15</sup>. From this model it becomes evident that a critical fibre length, designated  $L_c$ , is required if maximum fibre tensile stresses are to be achieved. Dow reports that  $L_c$  depends on the elastic and shear properties of the fibres and matrix.

The mechanism by which a fibre contributes its strength to a composite is one of shear<sup>4</sup>. Thus, for a given pair of materials, the length of fibre that is bonded to the matrix must be sufficient to support a shear stress that is equivalent to the tensile stress on the fibre.

Equating the shear load on the interface to the tensile load necessary to cause failure of the fibre gives the so-called critical aspect ratio,

$$\left(\frac{L_c}{d_f}\right): \frac{\pi d_f^2 \sigma_f}{4} = \pi d_f L_c \tau$$

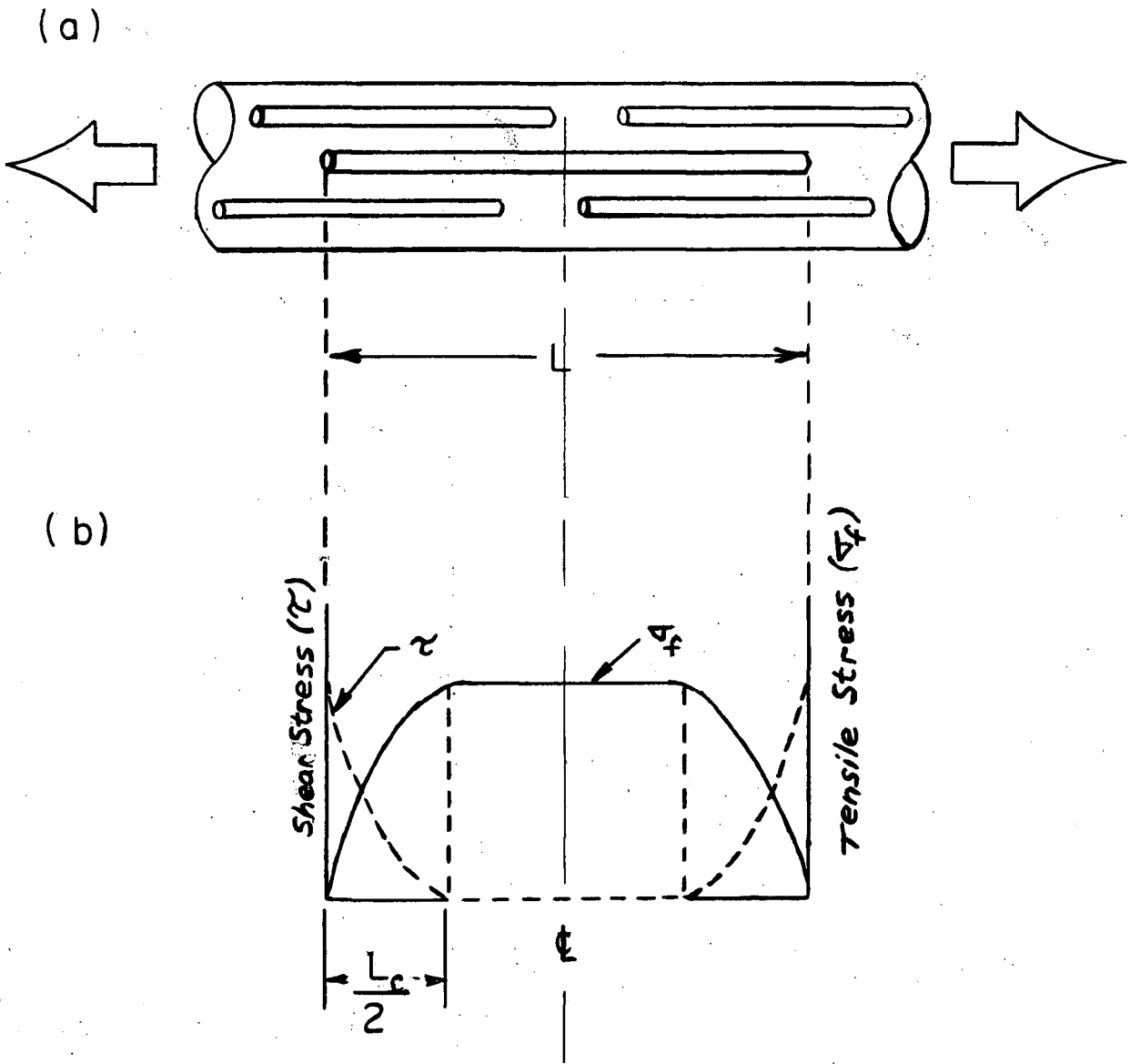


Figure 1

Schematic Relation Between Fibre Tensile Stress ( $\sigma_f$ ), Interfacial Shear Stress ( $\tau$ ), and Fibre Length ( $L$ )

or 
$$\frac{L_c}{d_f} = \frac{1}{4} \frac{\sigma_f}{\tau} \dots(5)$$

where  $d_f$  is the diameter of the fibre, and  $\tau$  is the shear stress at the interface.

Equation (1) predicts a linear relationship between strength and volume fraction of fibres. The fibres however, will carry the full predicted load only if  $L \gg L_c$ . For shorter fibres the proportion of the load carried by the fibres will be less and the results will be a weaker composite. This concept is shown schematically in Figure 2.

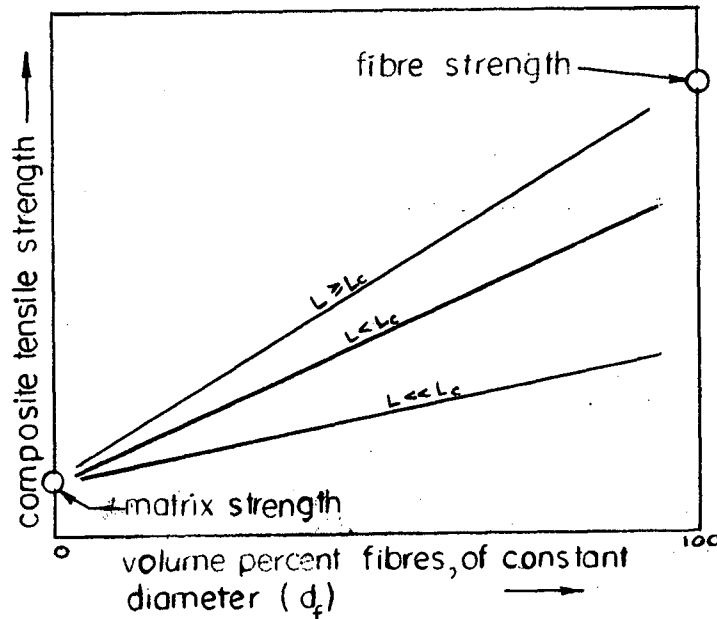


Figure 2. Relationship Between Composite Tensile Strength and Volume Per Cent Fibres for Various Fibre Lengths.

Figure 2, however, is over-simplified since the critical aspect ratio may be complicated by variations in interfibre spacing. The bond at the fibre-matrix interface restrains movement of the matrix relative to the fibre but the effect of this restraint is reduced as the distance from the interface is increased. Thus, there exists the possibility that the aspect ratio for a given fibre diameter will be lowered at high volume percentages of fibre and will become higher at low fibre contents.

Along these lines, Koppenaar and Parikh<sup>10</sup> state that the strengthening mechanism prevalent in the microstraining region of their silver-infiltrated felts is analogous in some respects, to grain boundary strengthening in polycrystalline metals. The fibres act as obstacles for slip, and dislocations pile up at the matrix-fibre interfaces. With increasing fibre density the available slip length decreases and a larger number of dislocations pile up for a given strain. The rate of work-hardening accordingly increases since larger stresses are required to force new dislocations into each pile-up. Parikh, using the Hall-Petch type of relationship:

$$\sigma_y = \sigma_0 + K d^{-1/2} \dots\dots(6)$$

and associating  $d$  with the average distance between fibres and  $\sigma_0$  with the fibre-independent portion of  $\sigma_y$ , has shown that varying the available slip length by changing the fibre density is quite analogous to changing the grain size in polycrystalline metals. The validity of equation (6) was established experimentally for the 0.2% yield strength in silver-infiltrated felts of mild steel, molybdenum, tungsten and martensitic stainless steel fibres.

The results of various workers are somewhat contradictory on the effect of wire diameter in reinforcing metallic systems. Jech et al.<sup>5</sup> found a size effect in tungsten-fibre-reinforced copper. Their results showed that the composites containing finer wires had higher strengths for a given volume fraction of the components. Cratchley<sup>7</sup> found that 0.002 in. diameter fibres gave stronger composites than 0.005 in. diameter fibres but attributed this strength increase to differences in wire-drawing conditions. The load transfer, for a given aspect ratio, was actually slightly less efficient for the thinner fibres but this was attributed to effects due to orientation.

Of the several methods used to produce fibre-reinforced composites, the infiltration technique has been used most widely. Sutton<sup>4,11</sup> has used vacuum infiltration to incorporate alumina whiskers in silver and aluminum. Jech et al.<sup>5</sup> and Kelly<sup>6</sup> have used infiltration techniques in their investigations of the tungsten wire-copper matrix system. Koppenaal and Parikh<sup>10</sup> also concentrated on infiltration as a means of producing metal-wire felts with a silver matrix.

Some other techniques which have been successfully employed to produce fibre-reinforced systems include: (a) the compacting and sintering of metallic powders around metallic and non-metallic fibres<sup>7,12</sup>; (b) the production of fibres of an intermetallic in situ in the matrix metal by suitable solidification<sup>6</sup> or heat treatment<sup>13</sup>; and (c) the working into wire of certain copper-iron alloys in which an excess of iron over the solid solubility limit in copper is present as iron dendrites in the original cast alloy<sup>14</sup>.

C. Scope

For the purpose of the present investigation it was felt that use might be made of the fact that the tensile strength of wires drawn from many metallic elements, increase with decreasing wire diameter (Figure 3).

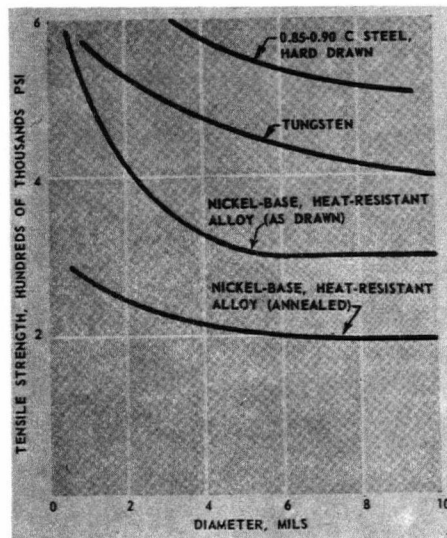


Figure 3. Tensile Strengths of Wires Drawn From Several Alloys. Reproduced from Roberts<sup>16</sup>.

Thus, if steel or iron wires could be incorporated into a ductile matrix and the resulting composite swaged and drawn to small sizes, a study could be made of the strengthening effect of very small diameter (whisker size and below) polycrystalline wires. Proper choice of a system would allow variations to be obtained in the relative properties of the matrix and the fibres by suitable heat treatments. In this way a study of the deformation behaviour of fibres and matrices of varying relative strengths could be made.

Two possible methods of producing the desired type of microstructure were visualized:

(a) Infiltration of a bundle of iron or steel wires with molten copper followed by swaging and drawing of the resulting composite, and

(b) Infiltration of porous, sintered, iron powder compacts with molten copper followed by swaging and drawing to produce fibrous iron in copper.

## II. EXPERIMENTAL PROCEDURE

### A. Materials

The high carbon steel wire used in this project was supplied by Precision Steel Warehouse, Inc., (Downers Grove, Ill.). The wire was of "spring grade" and was 0.012 inches in diameter. The chemical analysis, as received, was as follows:

Carbon	0.86 %
Manganese	0.44 %
Silicon	0.20 %
Sulphur	0.015 %

Armco iron powder, having nearly perfectly spherical particles was supplied by the Federal-Mogul, Power Plant Division of Ann Arbor, Mich. The nominal composition of the powder was:

Iron	99.94 % min.
Carbon	0.012 %
Manganese	0.017 %
Phosphorus	0.005 %
Sulphur	0.025 % max.
Silicon	Trace only.

Two screened fractions of the as-received powder were used in this work; (a) a minus 100 mesh (Tyler) plus 150 mesh fraction, and (b) a minus 325 mesh fraction of average particle size 25 microns.

The matrix metal for all composites was "Electrolyte Tough Pitch" copper, analyzing 99.92% copper with a nominal oxygen content of 0.04%.

An equilibrium diagram for the Fe-Cu system is given in Appendix I. This system was chosen for several reasons. It was felt that iron-copper composites would respond well to the required swaging and drawing operations, with the copper acting as a natural "lubricant" for deformation of the iron and steel. Furthermore, the system, after saturation of the iron with copper, would be heat treatable and thus the relative strengths of the matrix and fibre could be readily varied. The solubility of each component in the other is limited and well defined<sup>18,19</sup> and no intermetallic compounds are present in the system<sup>20</sup> which might detract from a sharp matrix-fibre interface. In addition, it was appreciated that the system satisfies the basic conditions necessary for infiltration in that (a) melting points of pure iron and copper are substantially different (1,527°C and 1,083°C respectively), (b) no phases of higher melting point exist which might obstruct the continuity of infiltration, and (c) iron is known to be wetted readily by liquid copper<sup>21</sup>.

## B. Composite Preparation

### 1. Wire Composites

Bundles of 0.012 inch diameter high carbon steel wire were infiltrated with copper using the following procedures:

(a) Wires of approximately 9 inches in length were cleaned in an aqueous solution containing 40 g.p.l.  $\text{Na}_2\text{CO}_3$ , 13 g.p.l.  $\text{NaOH}$ , 13 g.p.l.  $\text{Na}_2\text{PO}_4 \cdot 12\text{H}_2\text{O}$ , 13 g.p.l.  $\text{NaCN}$ , and 6 g.p.l.  $\text{Na}_2\text{SiO}_3$  at about 80°C.

(b) One-hundred and twenty wires were placed inside a copper tube measuring 8 inches long by 0.250 inches outside diameter. The wall

thickness of the tubing used was 0.040 inches.

(c) The resulting assembly was drawn through a 0.200 inch diameter hardened steel die to increase the closeness of packing and to aid in the alignment of the wires prior to infiltration.

(d) Infiltration was carried out in a closed-end, fused quartz tube of inside diameter slightly greater than the drawn steel wire-copper tube assembly. The fused quartz tube was so placed in a Glo-Bar furnace that all but the top one inch of the copper tube melted. The geometry of the system is as shown in Figure 4.

All infiltrations were performed at 1150°C for 9 minutes under fore-pump vacuum followed by 1 minute under a slight positive pressure of argon. (The argon treatment was found necessary to eliminate blistering the outside layer of copper.) Cooling to room temperature was done under a positive pressure of argon.

The resulting composite was essentially free of voids. The part of the copper tube which did not melt kept the wires together and in the center of the fused quartz tube during the time the remaining copper was in the molten state. The relatively thick coating of copper which resulted on the outside surface of the composite was desirable from the point of view of subsequent reduction by wire-drawing.

## 2. Powder Composites

Compacts of -100 +150 mesh Armco iron powder were infiltrated with copper using the following procedure:

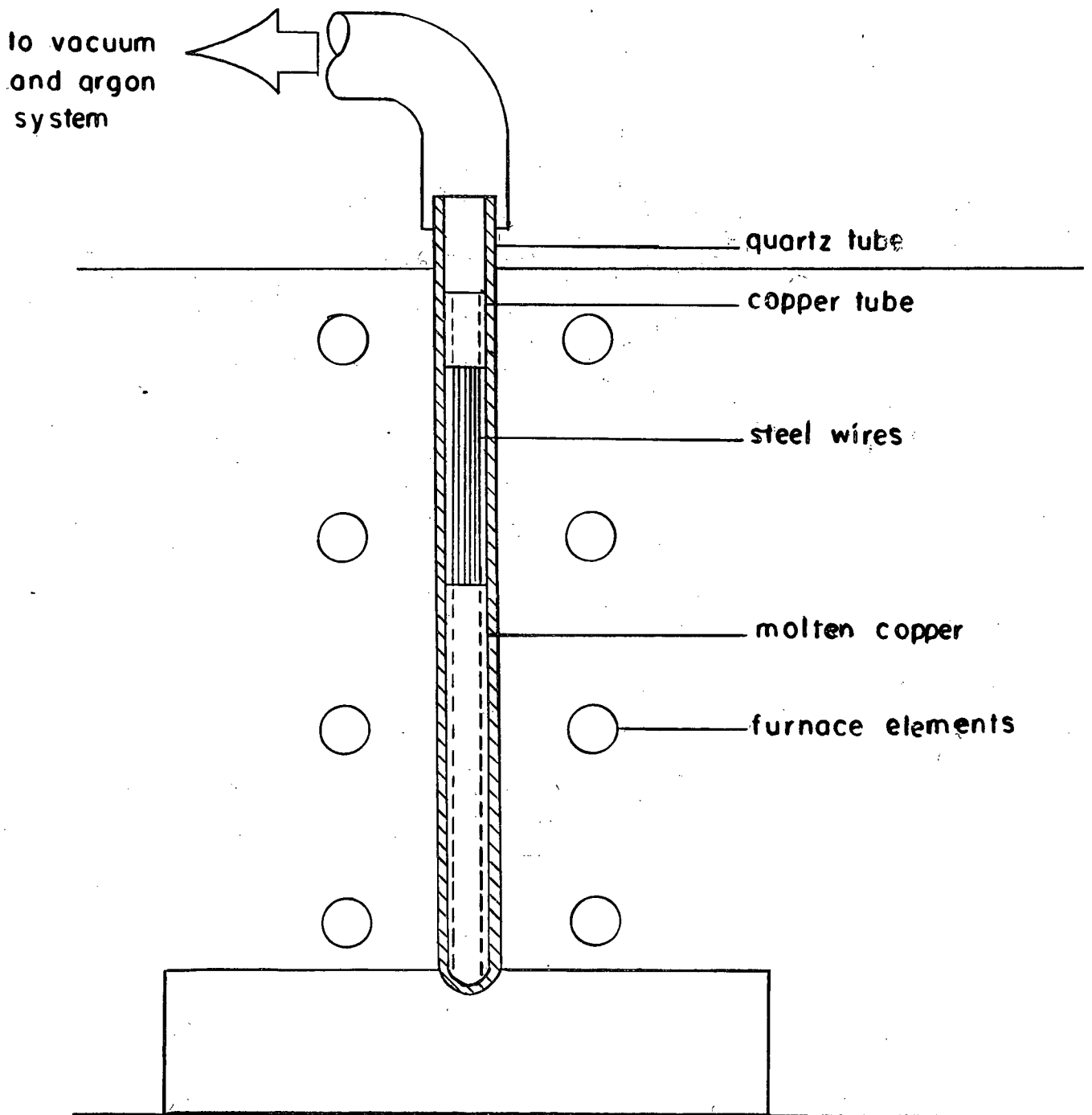


Figure 4 System For Infiltration of Steel Wire Bundles

(a) Powders were pressed hydrostatically in bags made from Gooch tubing, at a pressure of approximately 25,000 p.s.i.

(b) Sintering of green compacts was effected in 10 minutes at 1150°C under dry hydrogen.

(c) Infiltration for 10 minutes at 1110°C was carried out under fore-pump vacuum in a Vitreosil tube, providing an excess of copper over that needed to fill the voids in the iron skeleton. The technique used was developed by Krantz<sup>17</sup>.

This procedure yielded composites 3 to 4 inches long by 0.460 inches in diameter with the following characteristics:

- density of sintered iron skeleton  $74.0 \pm 2\%$  of theoretical
- density of infiltrated compact  $96.7 \pm 1\%$  of theoretical.

The composites were annealed for one hour at 680°C under dry hydrogen to ensure that the matrix was not supersaturated in iron; i.e. that the matrix was as ductile as possible for subsequent forming operations.

The procedure used for the -325 mesh Armco iron powder was essentially identical to that described above except that no pressure was used to prepare green "compacts". A tube of the loose powder was simply vibrated by tapping until no further change in volume was observed and the resulting mass sintered at 1150°C. Sintering in this case was done in a fore-pump vacuum.

The composites produced from -325 mesh powder had the following characteristics:

- density of sintered iron skeleton  $57.3\%$  of theoretical
- density of infiltrated compact  $96.5\%$  of theoretical.

C. Swaging and Drawing

The reduction in size of the wire and powder composites was carried out using the schedule shown in Table I.

TABLE I.

Swaging and Drawing Schedule

Original Diameter (in.)	Final Diameter (in.)	Operation	Annealing Treatment <sup>AA</sup>
0.460 <sup>A</sup>	0.270 <sup>A</sup>	Swaging	1 hr. at 680°C
0.270 (powder)	0.163	Swaging	1 hr. at 680°C
0.250 (wires)	0.126	Drawing	1 hr. at 680°C
0.163	0.098	Drawing	1 hr. at 680°C
0.126	0.077	Drawing	1 hr. at 680°C
0.098	0.060	Drawing	1 hr. at 680°C
0.077	0.046	Drawing	1 hr. at 680°C
0.060	0.035	Drawing	1 hr. at 680°C
0.046	0.028	Drawing	1 hr. at 680°C
0.035	0.021	Drawing	1 hr. at 680°C
0.028			

<sup>A</sup> Powder composites only.

<sup>AA</sup> All annealing treatments were carried out in a flow of dry hydrogen.

D. Heat Treating

Heat treatments were carried out on samples produced from iron powder composites in which the iron component had been completely saturated with copper at 1020°C. Six pieces of composite, each 3 inches long, were placed in a ceramic boat. Small alumina spacers were placed at each end to ensure that the wires were not in contact. Treatment was carried out in a small tube furnace under dry hydrogen gas. Heating for 15 hours at 1020°C to ensure alloy equilibrium was followed by cooling at various rates. The term "aircooled" will be applied to describe the rate of cooling which prevailed when the boat was withdrawn from the hot zone at approximately

3 inches per second to a point 12 inches distant where the temperature was below 200°C. The actual rate of cooling is estimated to be 120 to 180°C/second. Cooling by this method was entirely effected in dry hydrogen.

Several specimens were quenched in liquid nitrogen from the solution treatment temperature (1020°C). Specimens which had previously been solution treated and "aircooled" were, in this case, reheated to 1020°C for 20 minutes in a vertical tube furnace under a flow of dry hydrogen gas. The suspension was then cut, allowing the specimens to drop into a dewar of liquid nitrogen.

After solution treatment at 1020°C as before, one group of specimens was carburized using a commercial pack carburizing compound. Carburization for various times was carried out in a tube furnace open at both ends to the atmosphere. The pack carburizing compound was placed around the specimens in a ceramic boat and the furnace brought to a temperature of 920°C. Homogenization was carried out for 2 hours at 1020°C followed by "aircooling".

In addition to the heat treatments mentioned above several other annealing and cooling procedures were carried out on certain specimens. All such treatments were done in a small tube furnace under dry hydrogen. The actual procedure used for each specimen along with the pertinent results will be given in "Experimental Results".

#### E. Measurement of Fibre Concentration

The volume percentage of fibres present in the steel wire-copper matrix composites was calculated from cross-section micrographs using a random line technique. The length of line occupied by one phase was related to the total length of the line and averaged out over 12 random lines.

The volume percentage of fibres present in the composites made from iron powders was reasonably assumed to be equal to the density of iron in the as-sintered composites, since no detectable growth or shrinkage of the iron compacts accompanied infiltration.

#### F. Tensile Testing

All tests were carried out at room temperature on an Instron Tensile Testing machine using either wedge type grips or friction grips plus special universal mountings<sup>22</sup>. The cross-head speed in all tests was 0.01 inch/minute resulting in strain rates of  $0.0067 \text{ min}^{-1}$  for all the steel-wire composites and  $0.01 \text{ min}^{-1}$  for the composites made from iron powder. Per cent elongations reported are based on cross-head motion and thus are relative values, rather than absolutely accurate.

#### G. Metallography

An alternating polish-etch technique was found necessary to eliminate smearing of copper over the surfaces of metallographic specimens. Specimens to be viewed were mounted in "bakelite" and polished on five emery papers. The mounts were then lapped with 1 micron diamond powder in kerosene. Each lapping step was followed by etching with 4% picric acid in ethanol for 15 seconds. Four or five cycles were required to give the desired polish.

### III. RESULTS

#### A. Composites Made from High Carbon Steel Wire Bundles

##### 1. Structures

Obtaining fibre composites of the desired structure by infiltrating steel wire bundles with liquid copper proved to be only partially successful. A reduction of the composite diameter to a final specimen size of 0.022 inches (corresponding to individual steel wire diameters of 0.0023) was the maximum obtainable. Attempts to draw below this dimension led to cracking in the copper coating or random "necking" of the composite. It was originally felt that this problem was associated with imperfect alignment of the steel wires in the wire composites. However, in later work with powder composites difficulties were experienced in the same size range, and it became apparent that the drawing dies available were necessitating an unusually large reduction in one pass at the critical dimension.

Mechanical properties and structures of the wire composites were examined over the range of sizes which could be fabricated. Tensile testing was done on composite specimens of 0.100 inches diameter (individual wire diameter approximately 0.004 inches) and smaller. Micrographs of a cross-section and a longitudinal section of a typical specimen are shown in Figure 5. The relatively sharp matrix-fibre interface and the effect of annealing at 680°C are shown in Figure 6. As expected, the annealing treatment spheroidized the carbide in the steel wires.

The volume percentage of fibres present in these composites was measured using the method outlined in the Experimental Procedure. Over the range of specimen diameters investigated the volume per cent fibres

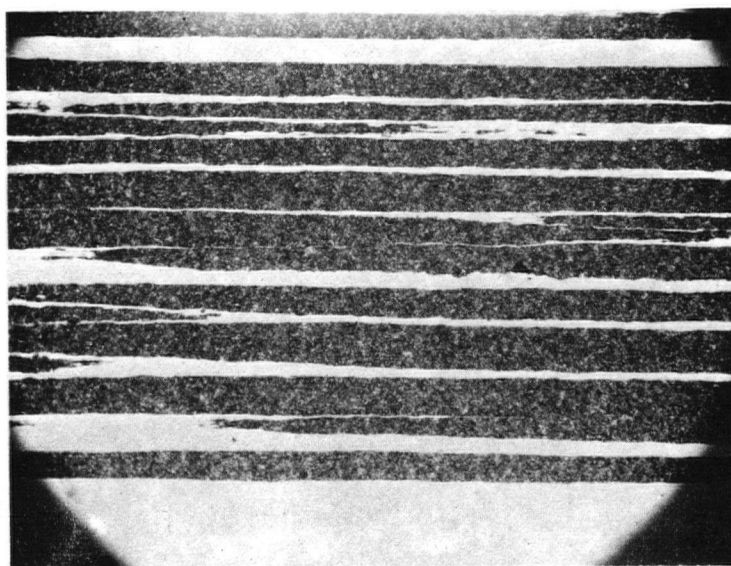
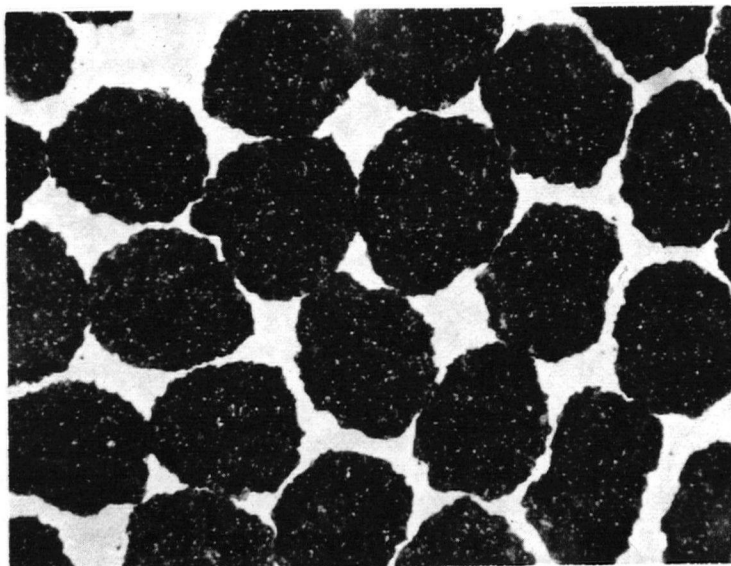


Figure 5. Cross-section (a) and Longitudinal Section (b) of Specimen W-1-A-6, approximate wire diameter 0.0033 inches, annealed 1 hour at 680°C, 2% nital etch, (a) X 200 (b) X 60.

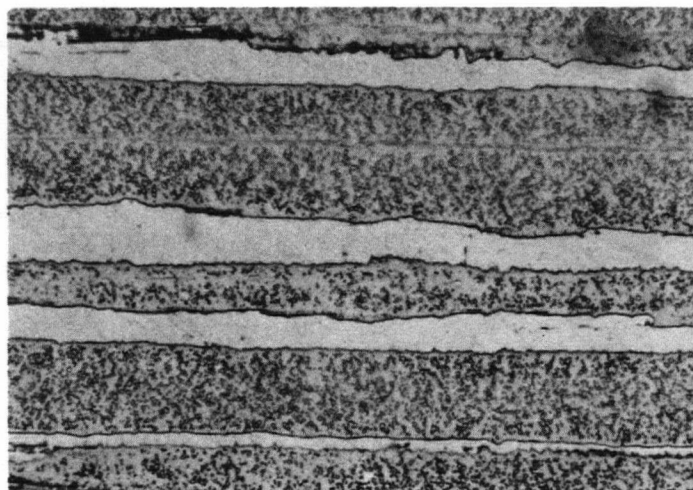


Figure 6. Effect of Annealing 1 hour at 680°C, Specimen W-1-A-11, picric etch, X 200.

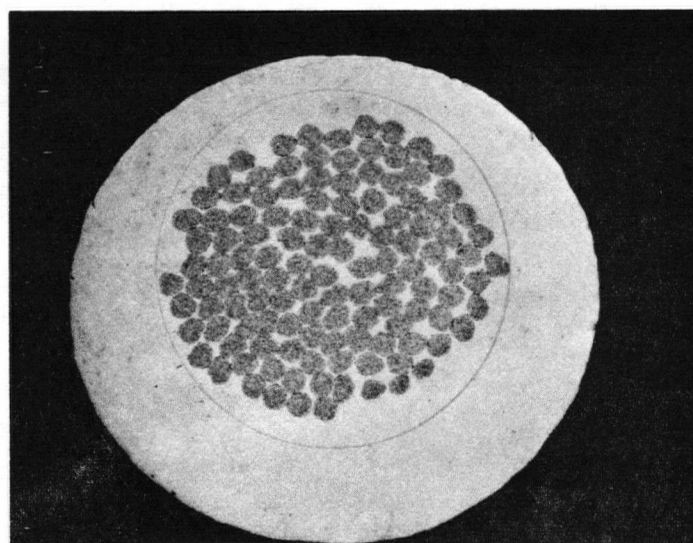


Figure 7. Distribution of Fibres in the Copper Matrix, Specimen W-1-12, nital etch, X 50.

remained virtually constant at 44.0%. This value was calculated using the complete cross-sectional area of the composite, i.e. including the relatively thick surface layer of copper. The fibres were closely packed at the centre of the composites (Figure 7). A more realistic packing fraction of fibres, based on measurements near the centre, is 0.75.

## 2. Size Effects

Tensile tests were made on annealed composite specimens in the size range 0.098 inches to 0.022 inches. Typical stress-plastic strain curves for two composites, W-1-A and W-3-A are shown in Figures 8a and 8b. These curves are plotted not to fracture, but to the ultimate tensile stress of the specimens.

Curves of composite yield stress and ultimate tensile stress versus specimen diameter for three different composites are shown in Figures 9 and 10. The diameter of the individual steel wires is also plotted on the abscissa.

It was observed that the load-elongation curves exhibited two apparent yield points; an initial yield point (designated  $Y_{P, \text{matrix}}$ ) which could possibly be attributed to the initiation of flow in the matrix, and a second yield point, (designated  $Y_{P, \text{composite}}$ ) which apparently corresponded to the start of plastic flow throughout the composite. The method of obtaining these two yield points from load-elongation curves is shown in Figure 11. (Figures 9 and 10 do not show the two yield points; they are plotted to start at the composite yield stress.) Figure 12 shows a plot of the "matrix yield stress" versus specimen diameter.

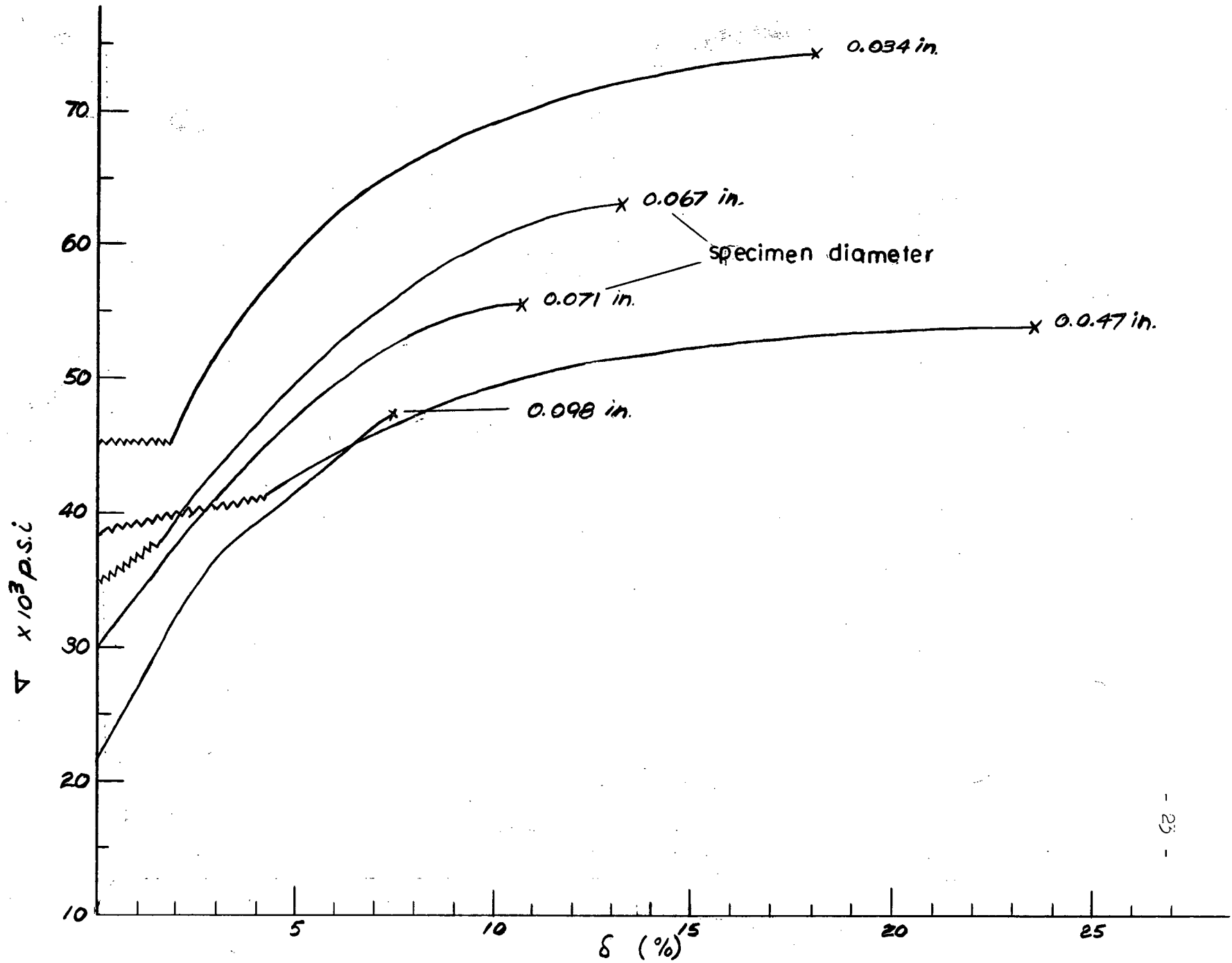


Figure 8a Typical Stress-Plastic Strain Curves, Composite W-1-A

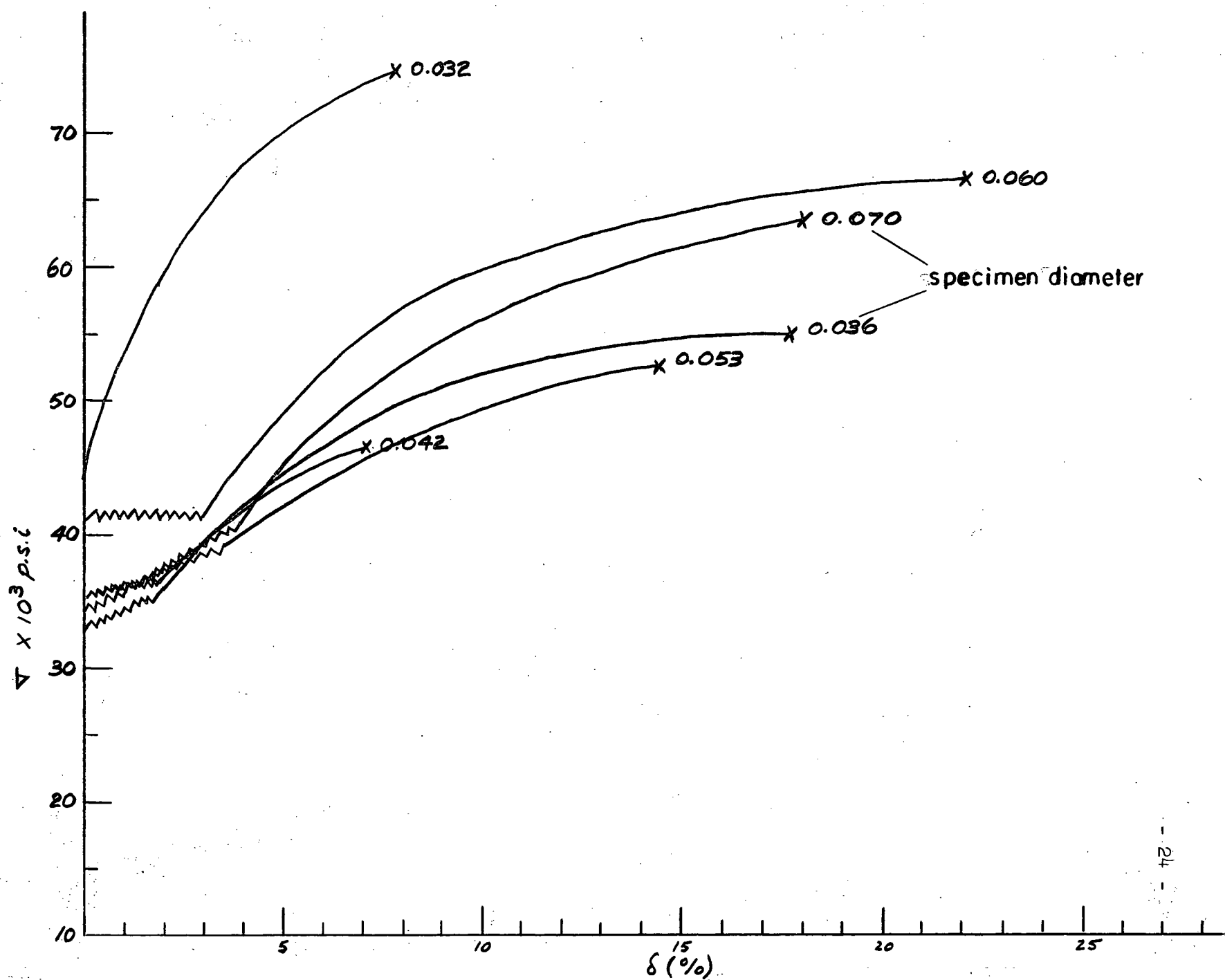


Figure 8b Typical Stress-Plastic Strain Curves, Composite W-3-A

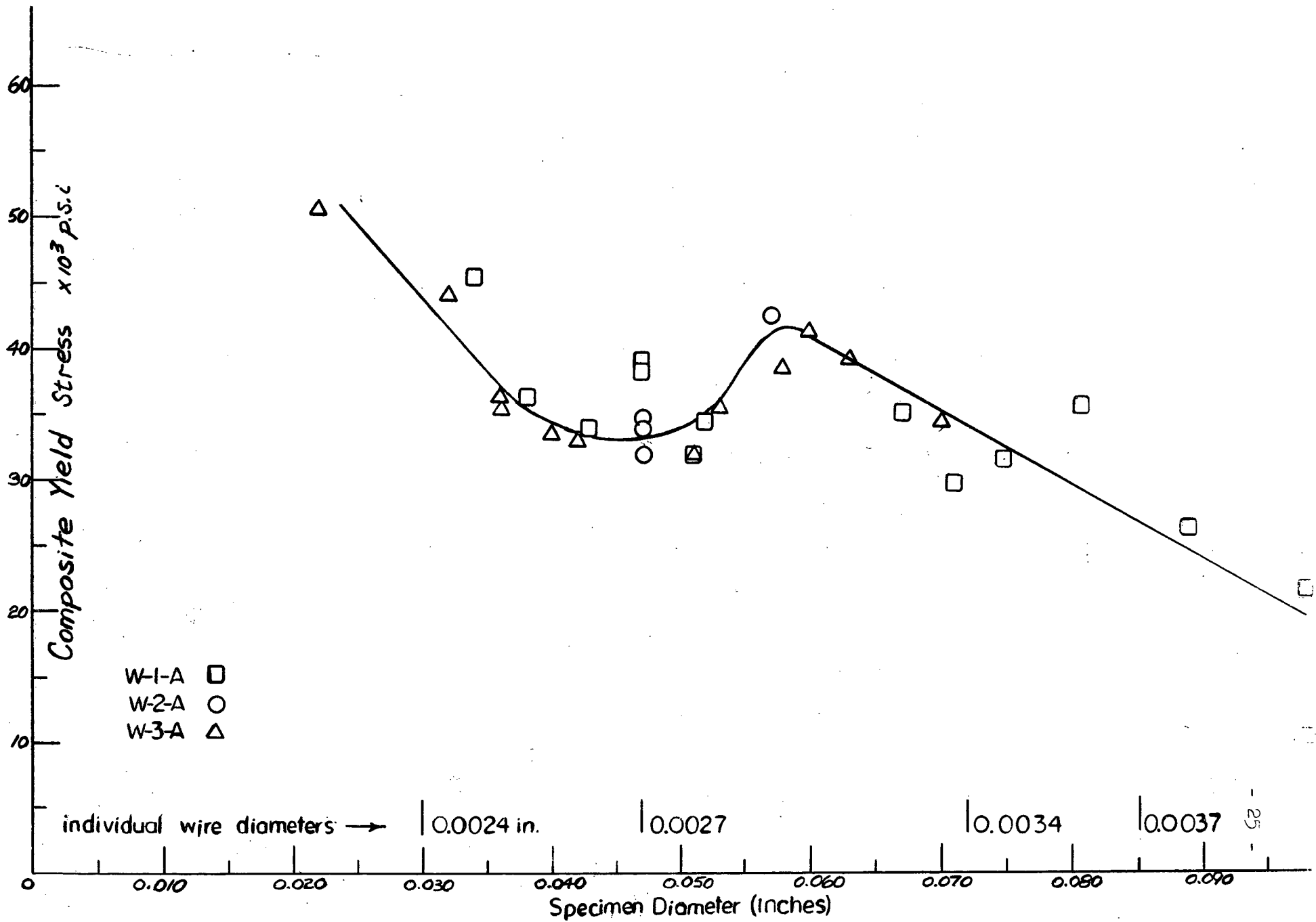


Figure 9 Composite Yield Stress Vs. Specimen Diameter-Composites W-1-A, W-2-A, W-3-A.

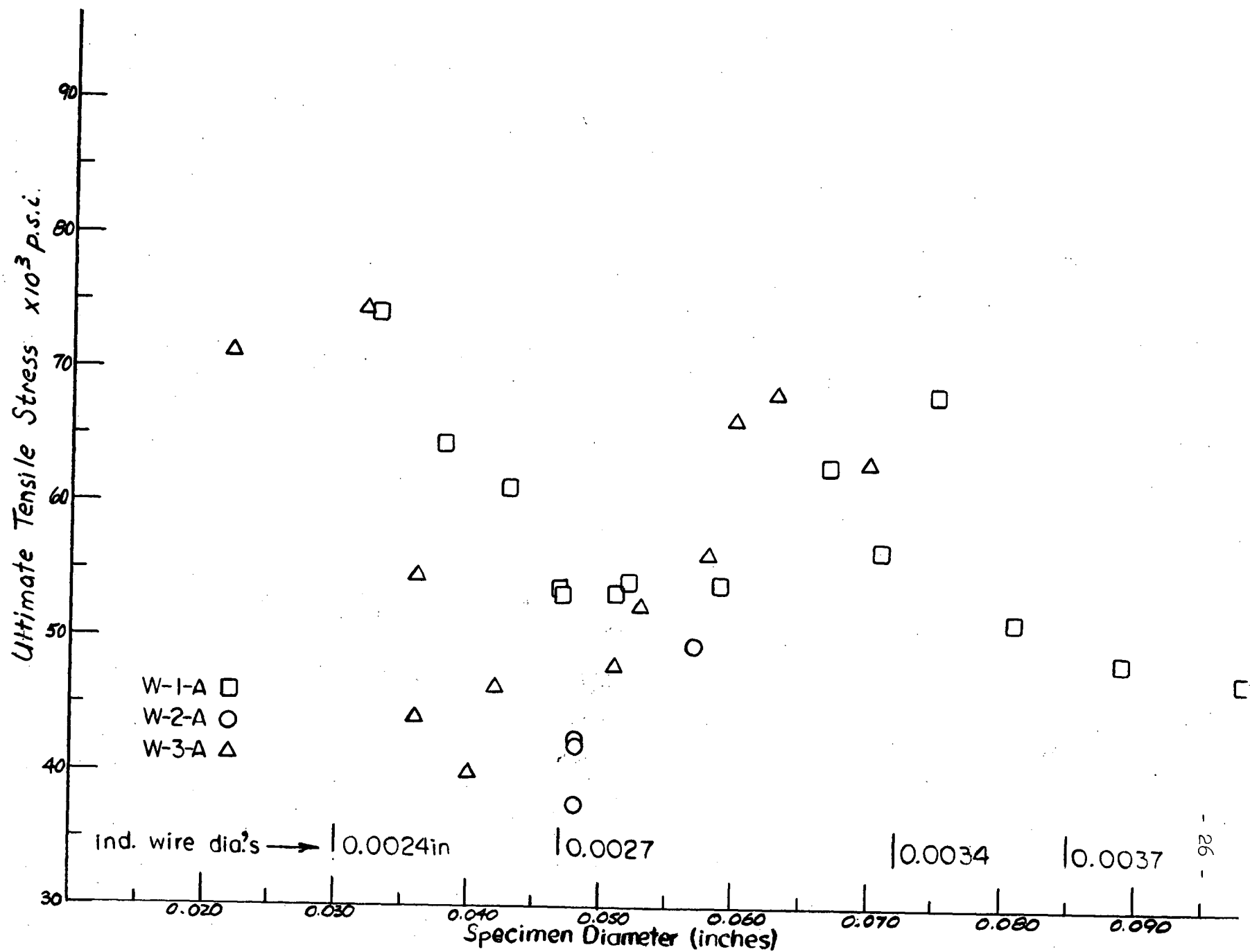


Figure 10 Ultimate Tensile Stress Vs. Specimen Diameter, Composites W-1-A, W-2-A, W-3-A.

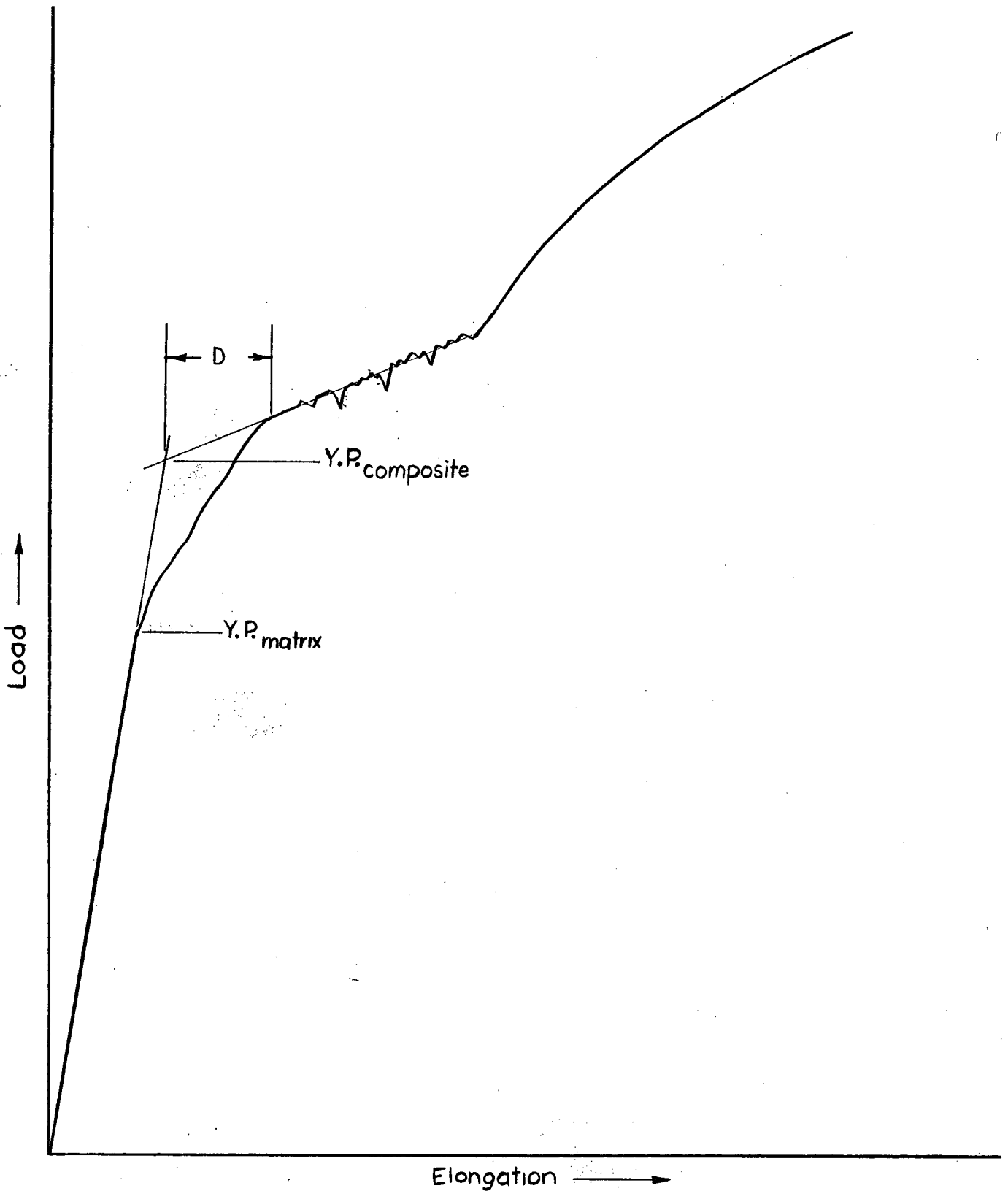


Figure II Method of Determining  $Y.P._{matrix}$  and  $Y.P._{composite}$  From Load-Elongation Curves.

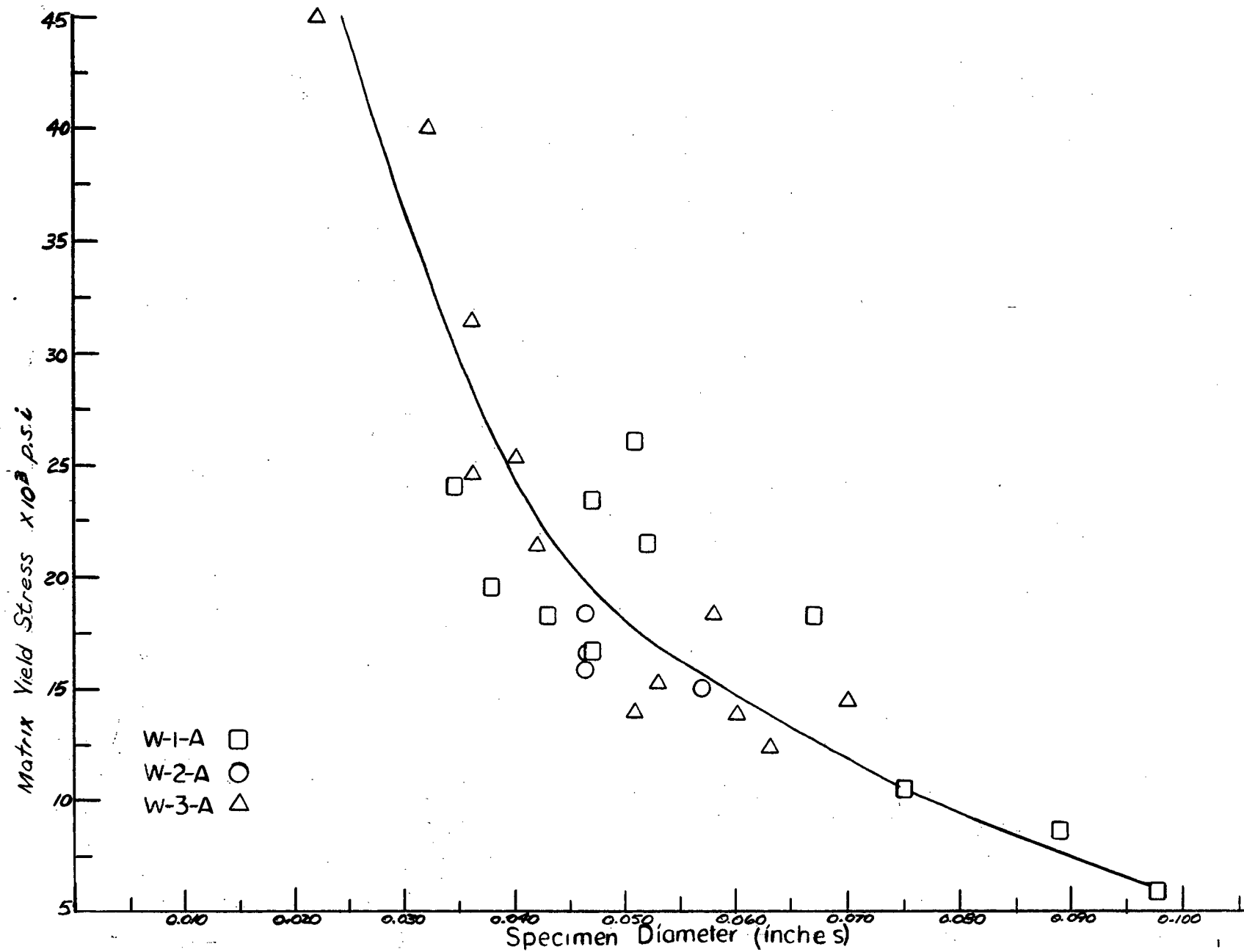


Figure 12 Matrix Yield Stress Vs. Specimen Diameter, Composites W-1-A, W-2-A, W-3-A.

An attempt was made to relate the thickness of copper on the outside of the composites to the characteristics of the load-elongation curves. To this end the distance D (in Figure 11) measured in percentage elongation is shown plotted versus specimen diameter in Figure 13.

Figures 8a and 8b indicate the heterogeneous yielding which was found to occur in certain specimens. Both the existence and extent of this behaviour were specimen size dependent in the manner shown in Figure 14. Discontinuous yielding was never observed with specimen diameters greater than 0.070 inches. The extent of the phenomenon increased to a maximum of about 4% (in per cent elongation over a 1 1/2 inch gauge length) at a specimen diameter of 0.047 inches and then diminished at smaller diameters as shown.

In an attempt to determine the work-hardening characteristics of the composites, values of n, the work-hardening exponent, in the empirical expression for the flow curve

$$\sigma' = K \epsilon'^n \dots\dots(7)$$

were calculated from the slopes of log-log plots of true stress ( $\sigma'$ ) versus true strain ( $\epsilon'$ ). The results (Table II) show no definite trends.

### 3. Studies of Heterogeneous Yielding

The appearance of heterogeneous yielding in certain specimens of composites made from the infiltration of steel wire bundles prompted further studies to determine the cause of the phenomenon.

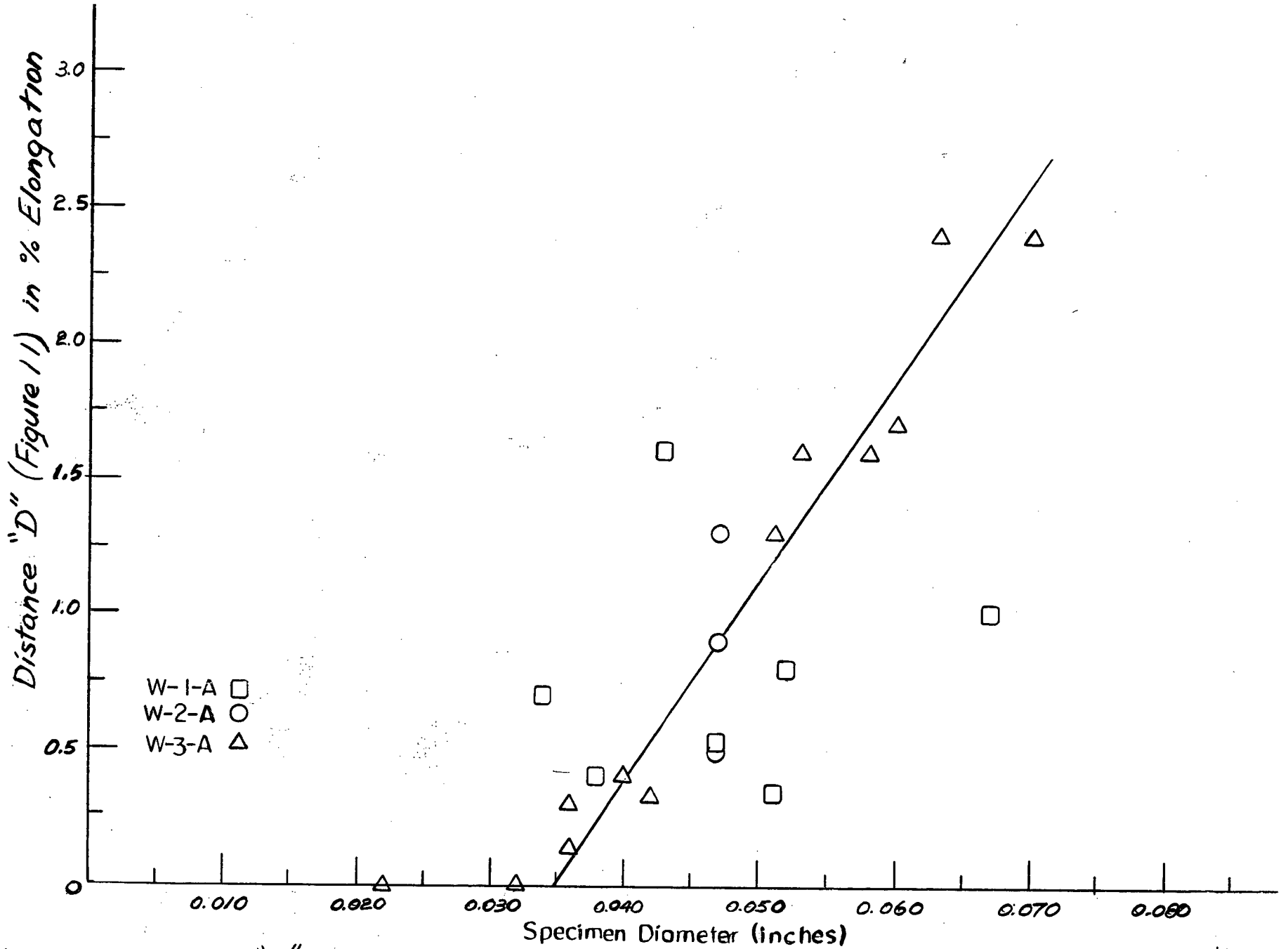


Figure 13 Distance "D" (Figure 11) Vs. Specimen Diameter

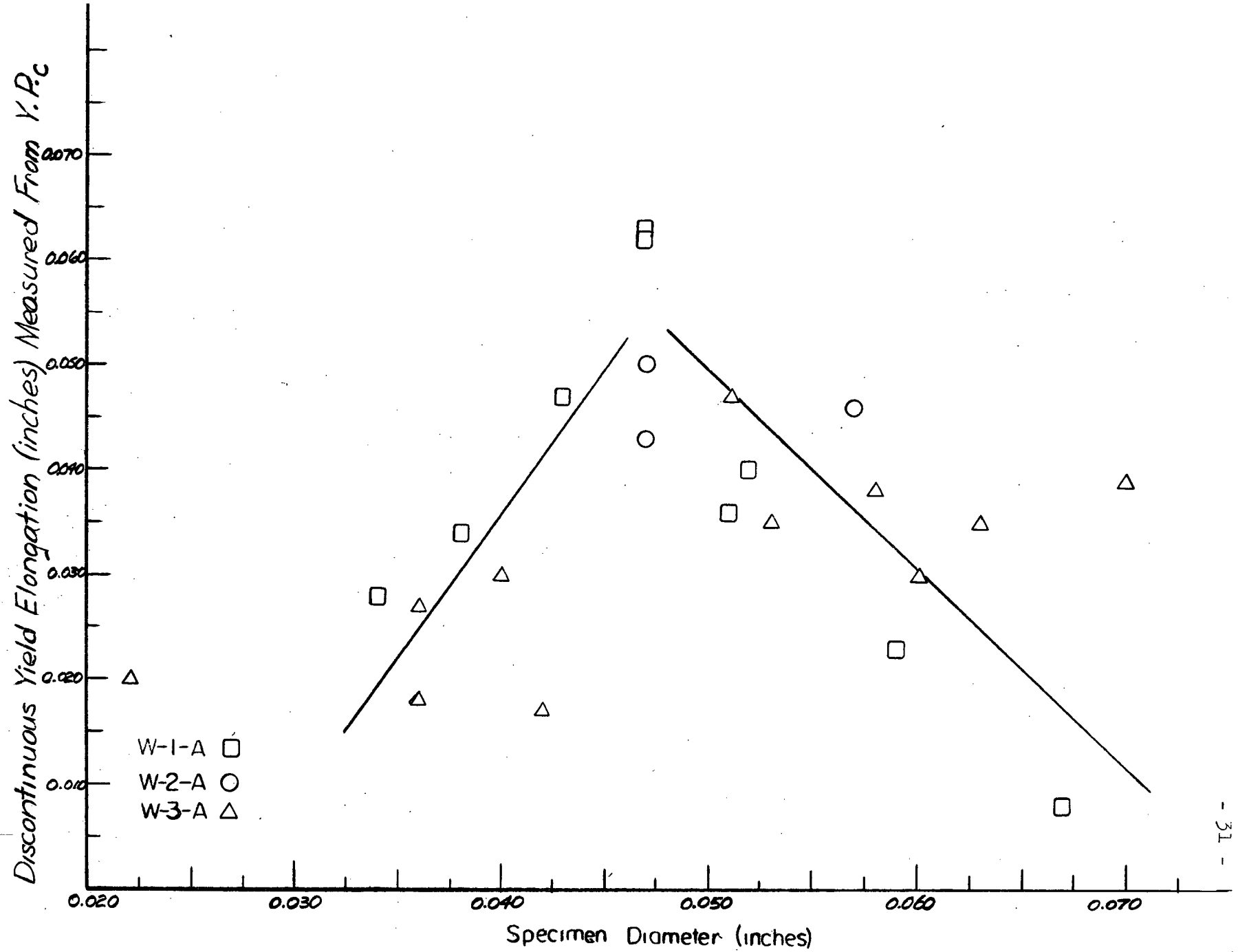


Figure 14 Discontinuous Yield Elongation Vs. Specimen Diameter.

TABLE II.

Work-Hardening Exponents

W-1-A		W-3-A	
Specimen Diameter	n	Specimen Diameter	n
0.098	0.297	0.070	0.150
0.089	0.177	0.060	0.169
0.081	0.125	0.053	0.104
0.075	0.213	0.032	0.217
0.067	0.179		
0.047	0.095		
0.034	0.174		

(a) Effect of Cold-Working - Cold working specimens by wire drawing prior to testing removed any trace of discontinuous yielding. Reductions in area of as little as 2.5% gave this result.

(b) Properties of Single Steel Wires - A single piece of the high carbon steel wire was annealed for 5 hours at 680°C and tested in tension. The same type of discontinuous yielding as found in the composites was found to occur but with somewhat smaller load drops, (Figure 15). It is also interesting to note that the strain hardening exponent of the annealed wire was found to be 0.167.

(c) Effect of Interrupted Loading - Several tests were stopped after discontinuous yielding was completed and the specimens unloaded. Loading was immediately re-applied and the tensile test was allowed to proceed to rupture of the specimen. The yield stress and work-hardening characteristics of these specimens were not affected by interrupting the loading.

(d) Effect of Strain Ageing - Several specimens at a size exhibiting the maximum amount of discontinuous yielding, i.e. 0.047 inches, were given strain ageing treatments. The specimens were strained until uniform deformation and work-hardening had commenced, and were then unloaded as in section (c) above. The samples were then aged for either 1/2 or 1 hour at 200°C followed by retesting. The effect of ageing on the matrix and composite yield stresses is summarized in Table III.

A discontinuous yield region was not resolvable in specimens aged for 1/2 hour but was definitely present in specimens aged for 1 hour. Approximately 70% of the original extent of discontinuous yielding had

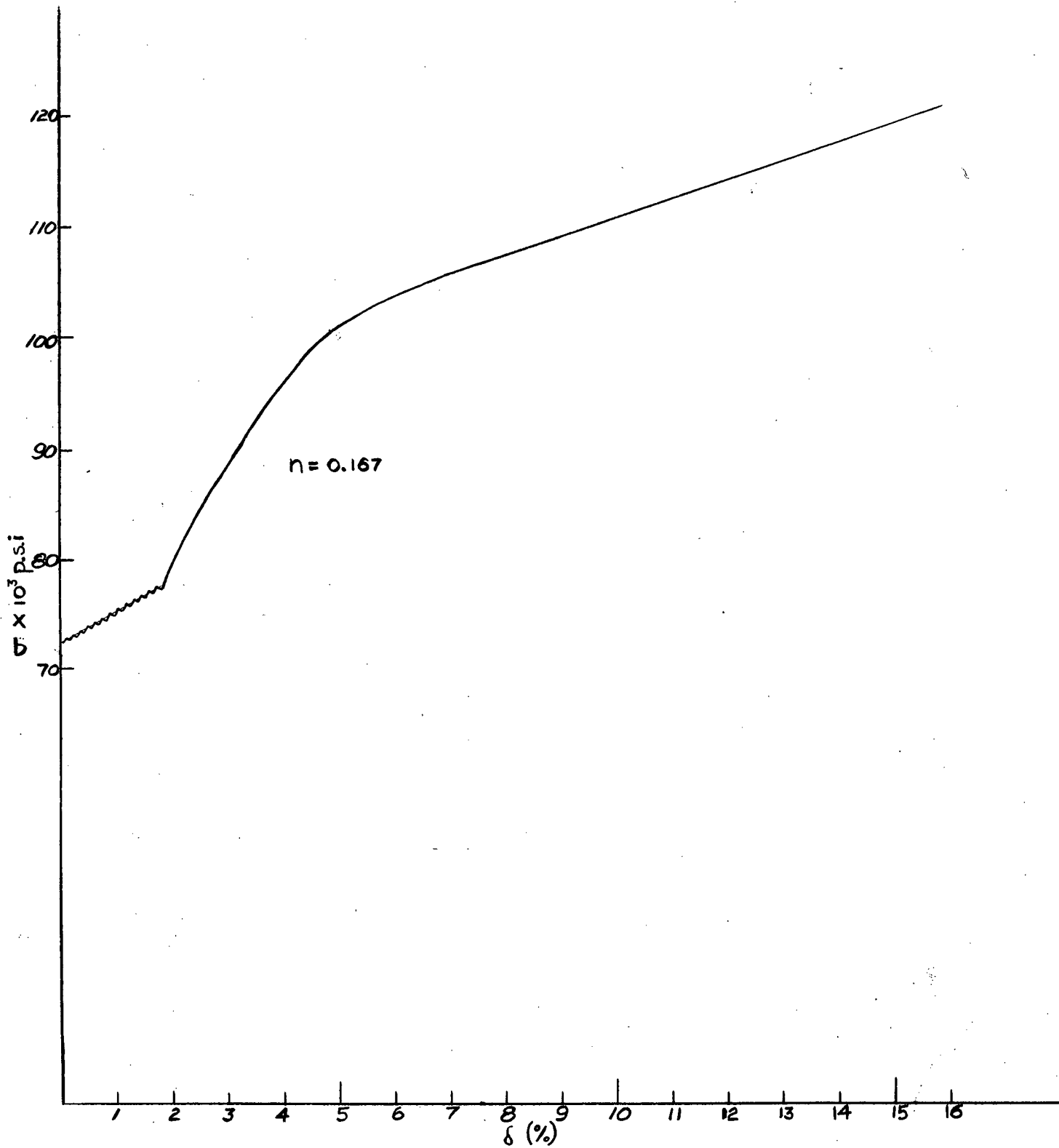


Figure 15 Stress-Plastic Strain Curve For Single Steel Wire, Diameter 0.049in, Annealed 5 hrs at 680°C.

returned, but with smaller load drops.

TABLE III.

Strain Ageing

Treatment		Y.S.M.	Y.S.c
1/2 hour at 200°C	Before Ageing	13,300 p.s.i.	34,500 p.s.i.
	After Ageing	20,000	43,000
1 hour at 200°C	Before Ageing	15,900	39,500
	After Ageing	21,400	41,500

(e) Observations During Loading - The surface of several specimens was polished with 4/0 emery paper and then observed during a tensile test. Deformation bands appeared at random points along the gauge lengths of the specimens, simultaneously with sudden load drops on the load-elongation curve. Continued loading caused the deformation bands to widen visibly until they interacted with each other. A shadowgraph of such a specimen is shown in Figure 16. The deformation bands are barely discernible at the perimeter of the specimen. The arrows indicate observed direction of deformation front motion.

B. Composites Made From Sintered Armco Iron Powder

1. Structures

The product of infiltrating pure iron powder skeletons with liquid copper followed by fabrication to produce fibrous iron in a copper matrix proved to be more interesting and more useful than that obtained from steel wire bundles. One advantage of the powder composites was that

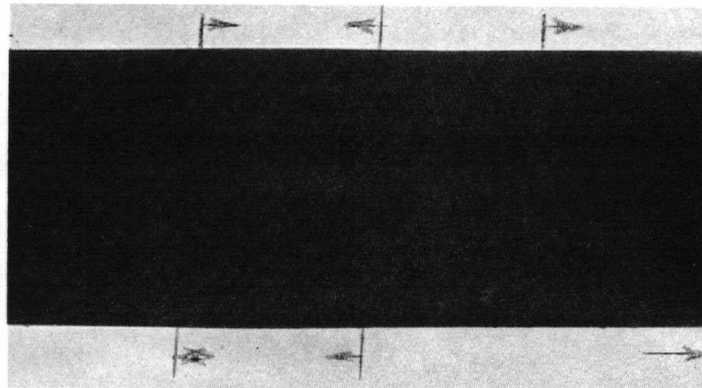


Figure 16. Deformation Bands on Polished Surface of Specimen W-4-L, X 30.

complications due to carbon and its partial depletion during annealing treatments were not present. Additionally, it was convenient to obtain much finer fibres by the powder approach.

Photomicrographs of some powder composites after drawing are shown in Figure 17. The materials shown were made from the two different powder fractions -100 +150 mesh and -325 mesh. Metallographic measurements on composite specimens of diameter 0.035 inches gave, for the average diameter of the fibres (a) 10 microns for the coarser powder composites and (b) approximately 2 microns for the finer powder composites. The probability that a fibre would lie in the plane of polishing over its entire length was negligible. Consequently, metallographic measurements could not be expected to give an accurate indication of the lengths of fibres. However an estimate of fibre lengths can be made from their diameters, as will be discussed later.

## 2. Size Effects

Tensile tests were done on -100 +150 mesh powder composites at various stages of reduction to determine the effect of specimen and fibre diameter in much the same way as for the steel wire composites. Typical stress-plastic strain curves for some specimen sizes are shown in Figures 18a and 18b. Plots of ultimate tensile stress and composite yield stress versus specimen diameter are shown in Figures 19 and 20. Only a slight increase in strength with decreasing composite diameter was suggested by the data.

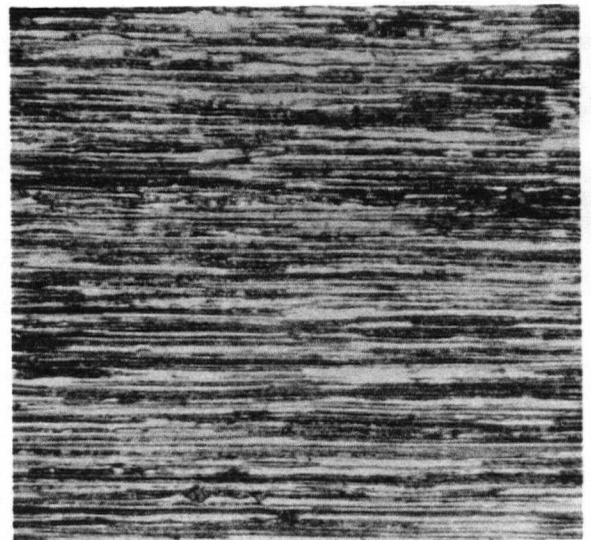
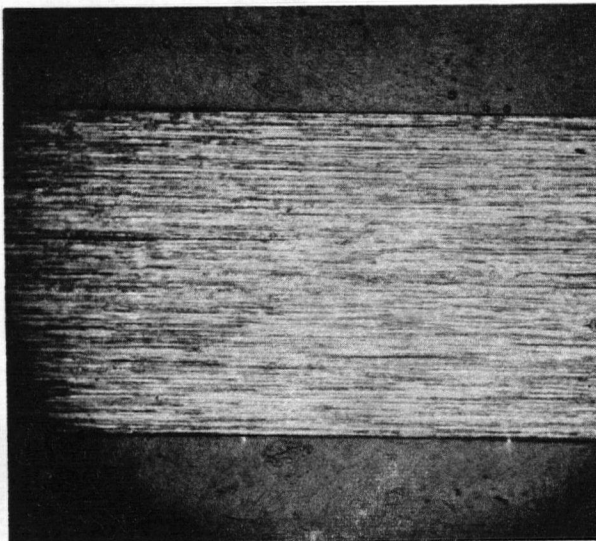
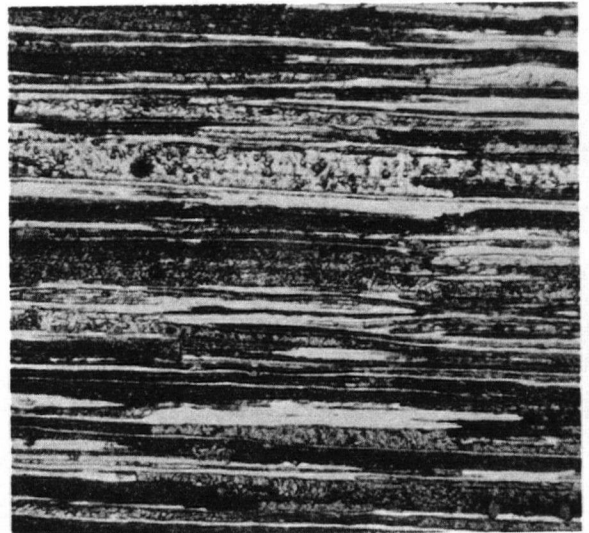
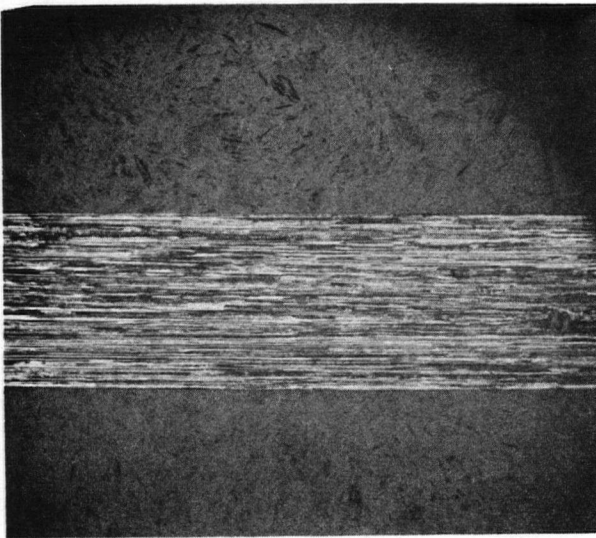


Figure 17. Sections through Iron Powder Composites, Specimen diameter 0.035 inches, annealed 1 hour at 680°C, 2% nital etch. (a) -100 +150 mesh, X 26, (b) -100 +150 mesh, X 200, (c) -325 mesh, X 47, (d) -325 mesh X 200.

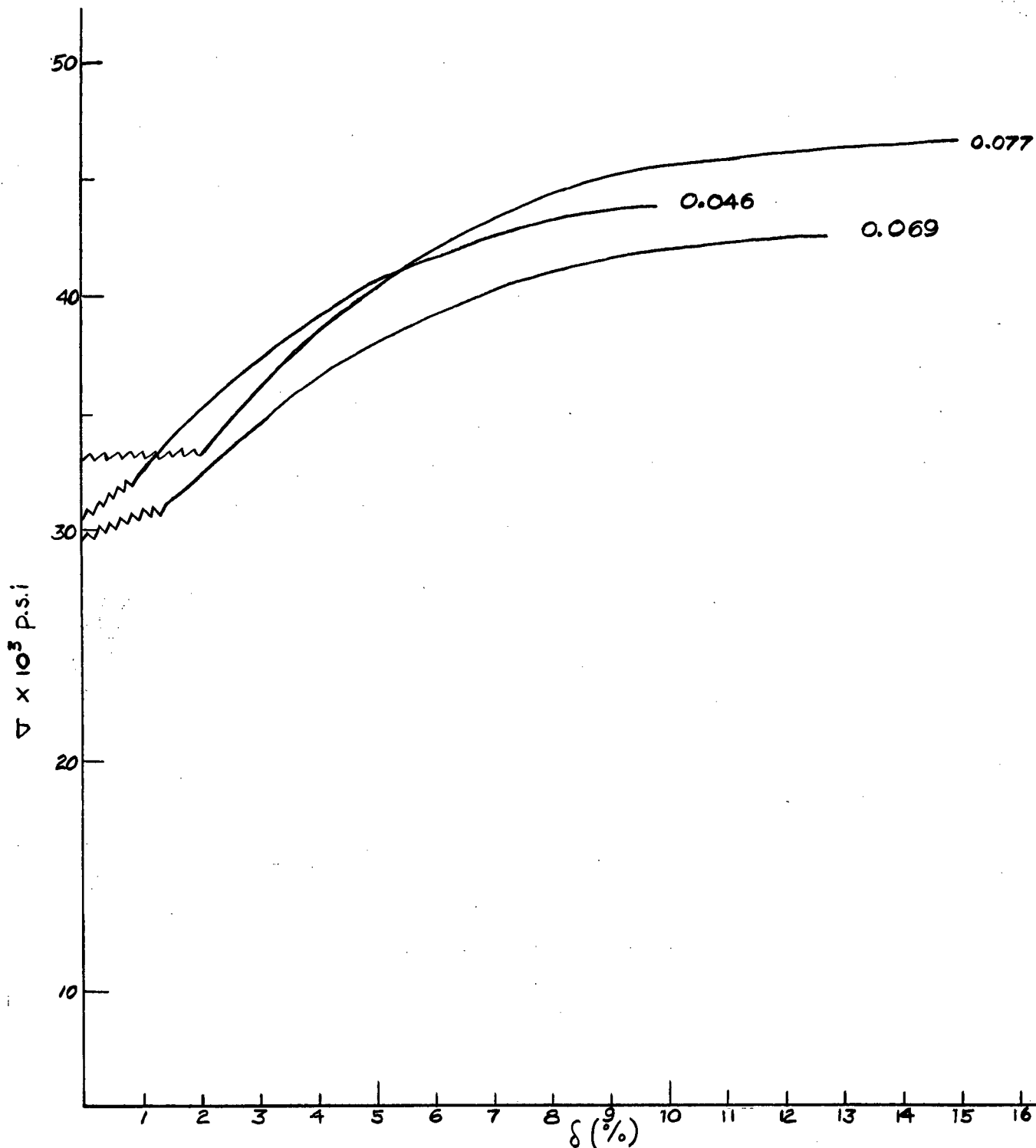


Figure 18 Stress-Plastic Strain Curves For Various Specimen Diameters  
- 100+150 Mesh Powder Composites

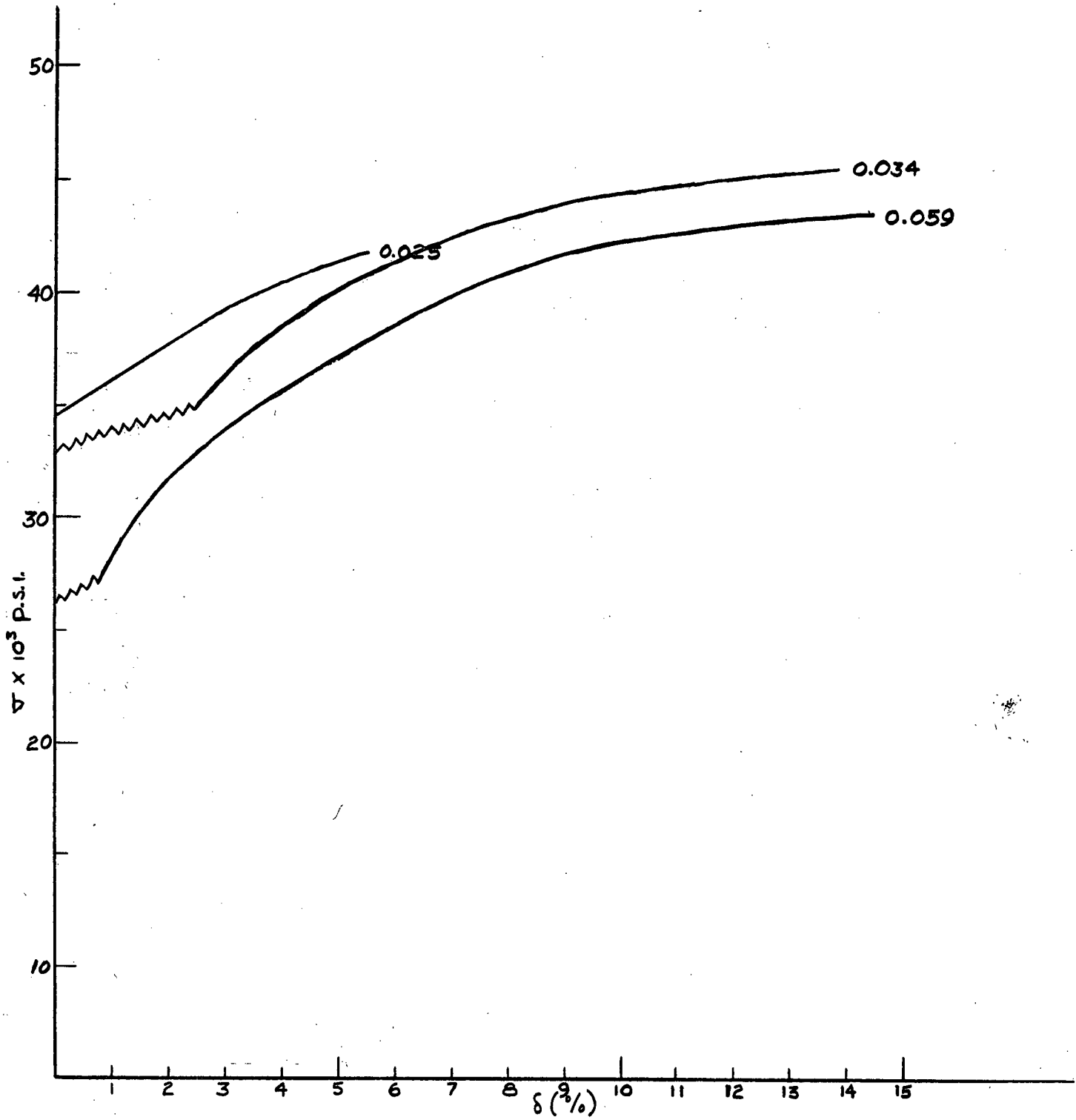


Figure 18 Continued

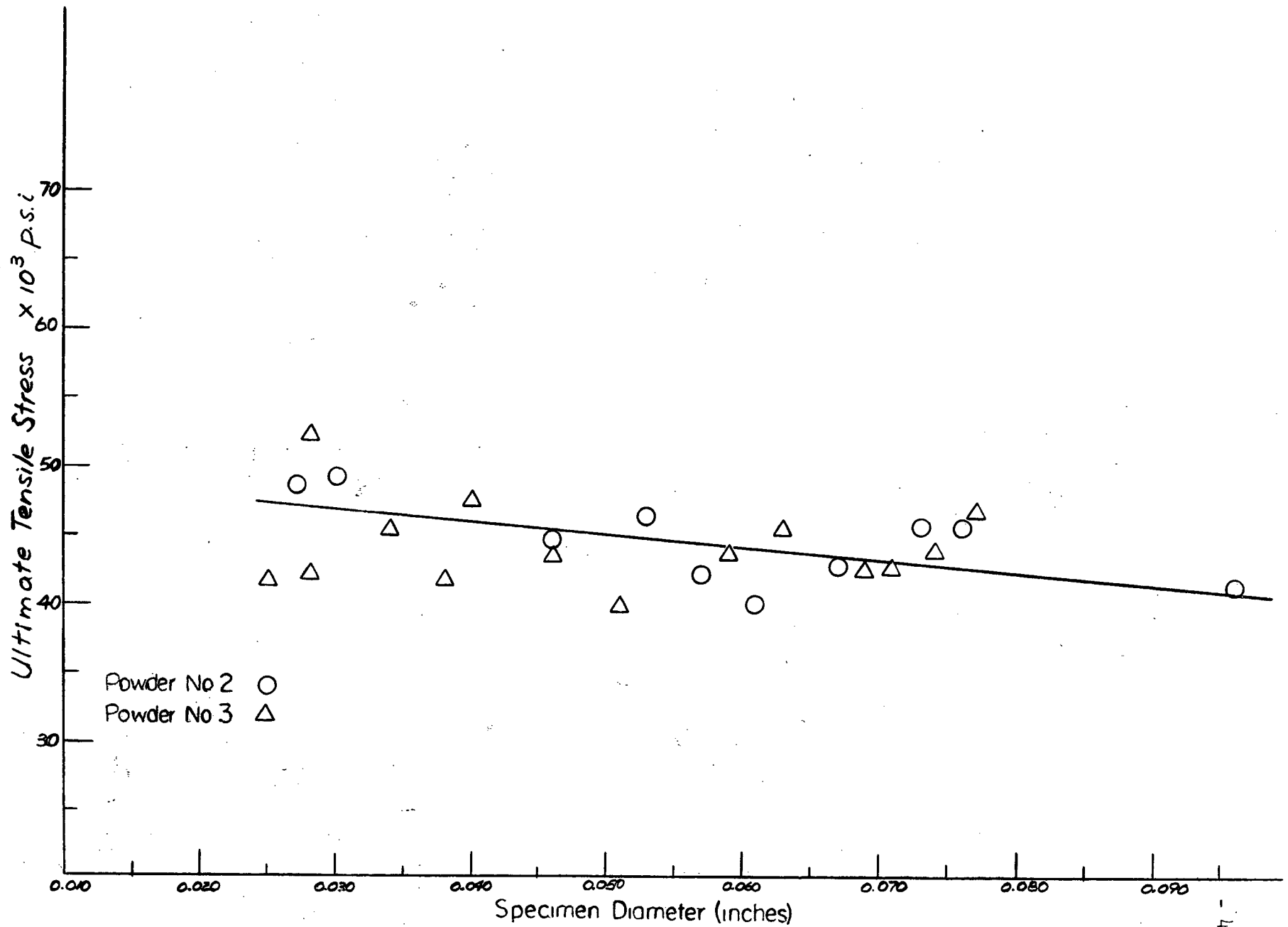


Figure 19 U.T.S. Vs. Specimen Diameter, -100+150 Mesh Powder Composites

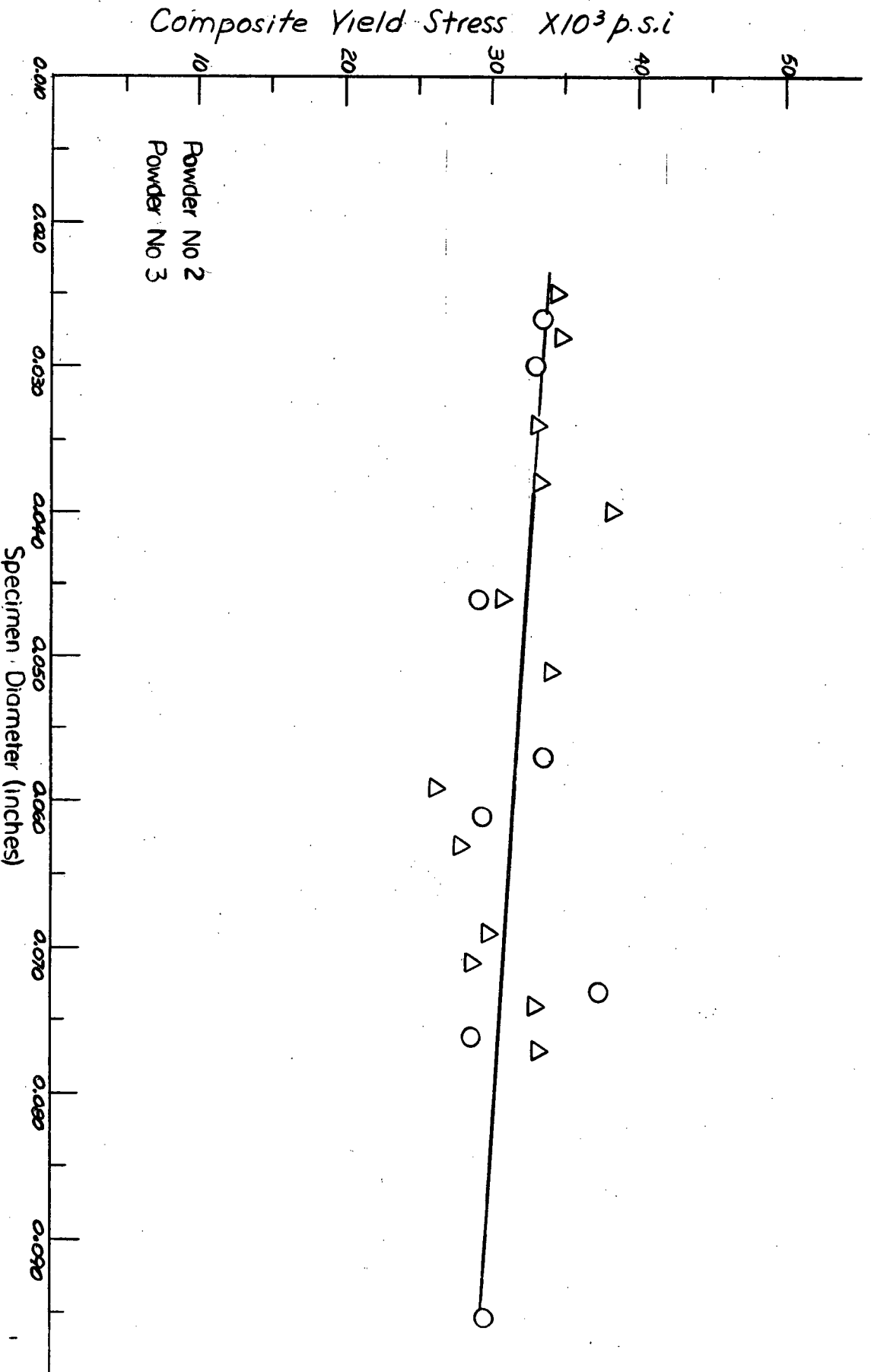


Figure 20 Composite Y.S. Vs. Specimen Diameter, -100+150 Mesh Powder Composites

The load-elongation curves for all the powder composites were such as to indicate a single yield point rather than two as observed for the steel wire composites. Consequently this one yield point has been designated as  $Y P_{\text{composite}}$ .

Work-hardening exponents were calculated at various specimen diameters. If heterogeneous yielding was present the work-hardening exponent was calculated from that part of the flow curve immediately following completion of discontinuous yielding. For this purpose, the point of zero plastic strain was arbitrarily taken as being at the end of the discontinuous yielding region. The results are tabulated in Table IV.

TABLE IV.

Work-Hardening Exponents

<u>Powder No. 3 Specimen Diameter</u>	<u>n</u>
0.077 inches	0.115
0.069	0.117
0.059	0.149
0.046	0.145
0.034	0.100
0.025	0.121

As in the case of the steel wire composites, no definite trend in these values was apparent.

3. Heterogeneous Yielding

Discontinuous yielding was sometimes observed with powder composites. The extent of the phenomenon was markedly less than that obtained in steel wire composites and seemed to be virtually random in its dependence on

specimen diameter. Cold working of the powder specimens (as little as 2%) prior to testing eliminated any trace of discontinuous yielding.

#### 4. Heat Treatments on Saturated Iron-Powder Composites

Various heat treatments were carried out on the powder composites. Specimens were initially solution treated to saturate the iron fibres with copper at 1020°C and were then cooled at varying rates. Several different secondary treatments were also applied in certain cases. A carburizing treatment was given to one series of specimens in an attempt to ascertain the possible effect of carbon additions to the iron fibres.

(a) Results with -100 +150 mesh powder composites - All the following results are from specimens which had been solution treated under dry hydrogen for 15 hours at 1020°C, then cooled and further heat treated as indicated. The elongations reported are as measured from the yield point to the ultimate tensile stress. The gauge length used in all cases was 1 inch.

(i) "Aircooled" (120 to 180°C per second)

Specimen Diameter	U.T.S. lbs/in <sup>2</sup>	Y.S. lbs/in <sup>2</sup>	Elong. %
0.035	138,000	108,300	12.2
0.035	140,500	110,200	14.1
0.035	141,500	119,500	11.7

A photomicrograph of the corresponding structure is shown in Figure 21.

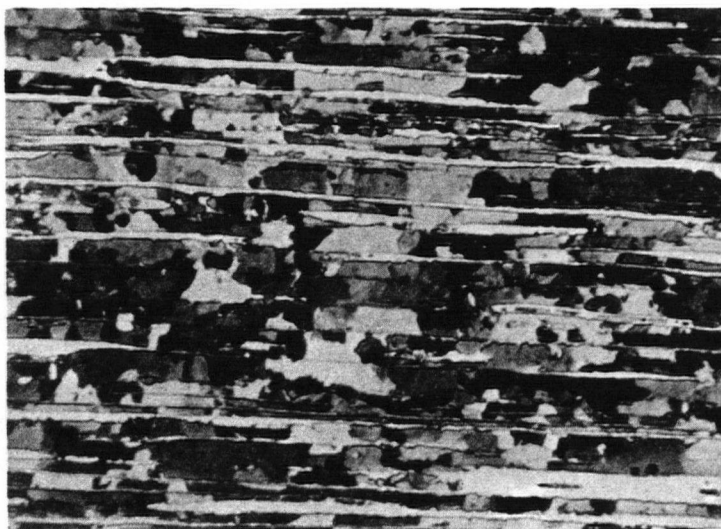


Figure 21. Photomicrograph of -100 +150 mesh Powder Composite  
"aircooled" from 1020°C, 2% nital etch, X 240.

(ii) "Aircooled" and Reheated 1 hour at 400°C

Specimen Diameter	U.T.S. lbs/in <sup>2</sup>	Y.S. lbs/in <sup>2</sup>	Elong. %
0.035	135,700	123,500	13.0
0.035	138,000	127,700	13.0

No discontinuous yielding was observed in specimens from (i) or (ii) above.

(iii) "Aircooled" and Reheated 1 hour at 750°C

Discontinuous yielding occurred in these specimens.

Specimen Diameter	U.T.S. lbs/in <sup>2</sup>	Y.S. lbs/in <sup>2</sup>	Elong. %	Discontinuous Yield Elong. %
0.035	59,600	47,800	22.7	2.2
0.035	61,500	49,000	23.1	1.8

(iv) "Aircooled" and Cold Drawn

Several specimens were saturated, "aircooled" and drawn cold to obtain an additional 40% reduction in area. They were then annealed 1 hour at 250°C to induce recrystallization of the matrix.

Specimen Diameter	U.T.S. lbs/in <sup>2</sup>	Y.S. lbs/in <sup>2</sup>	Elong. %
0.035	163,000	56,200	5.8
0.035	173,000	55,100	5.2
0.035	178,000	79,000	5.2
0.035	173,000	64,300	5.1

(v) "Aircooled" Reheated at 400°C, and Cold Drawn

Several specimens were saturated, "aircooled", reheated 1 hour at 400°C, drawn an additional 40% reduction in area and annealed 1 hour at 250°C.

Specimen Diameter	U.T.S. lbs/in <sup>2</sup>	Y.S. lbs/in <sup>2</sup>	Elong. %
0.035	175,500	88,400	4.4
0.035	179,500	72,800	5.4

(vi) Quenched in Liquid Nitrogen and Aged at Room Temperature

Saturated and "aircooled" specimens were reheated to 1020°C for 20 minutes followed by rapid quenching in a bath of liquid nitrogen (-196°C). The specimens were then allowed to reheat to room temperature, and were held there for various times prior to testing. All specimens were found to be magnetic at -196°C.

Specimen Diameter	Aging Time	U.T.S. lbs/in <sup>2</sup>	Y.S. lbs/in <sup>2</sup>	Elong. %
0.035	0 hrs	107,700	84,200	1.0
0.035	0	104,500	86,200	1.4
0.035	3	120,800	94,100	6.3
0.035	24	121,000	106,700	6.0
0.035	100	133,000	118,500	5.7
0.035	300	130,500	76,000	2.4

(vii) Slow cooled from 1020°C

Two specimens were sealed off in a fused quartz tube under vacuum. The sealed tube was placed in the centre of a resistance-heated box furnace and surrounded by refractory bricks. Solution treatment was carried out at 1020°C for 15 hours and then the power supply to the furnace was shut off. The maximum rate of cooling experienced between 1020°C and 25°C, was 2°C/minute.

Specimen Diameter	U.T.S. lbs/in <sup>2</sup>	Y.S. lbs/in <sup>2</sup>	Elong. %	Discontinuous Yield Elong. %
0.035	50,800	39,200	28.0	2.4
0.035	49,900	39,300	26.8	2.9

Representative stress-plastic strain curves for the various heat treatments are shown in Figure 22. The work-hardening exponents are shown with each curve.

(b) Results with -325 mesh Powder Composites - During the solution treatment of all composites produced from -325 mesh iron powder, a marked loss of continuity in the fibres was found to occur. The resulting structure (shown in Figure 23) was considerably different from that of composites made from wire or coarser powders. It is likely that disintegration of the fibres in fine powder composites is associated with the relatively high volume per cent of copper (initially not saturated with iron at 1020°C) which might be capable of dissolving an appreciable fraction of the iron present during solution treatment. Because of the discontinuity of many of the fibres in these composites, it may not be justified to compare the results which follow with those obtained for the coarser powder materials.

(i) "Aircooled"

Specimen Diameter	U.T.S. lbs/in <sup>2</sup>	Y.S. lbs/in <sup>2</sup>	Elong. %
0.035	122,700	114,000	12.0
0.035	120,700	111,000	12.6

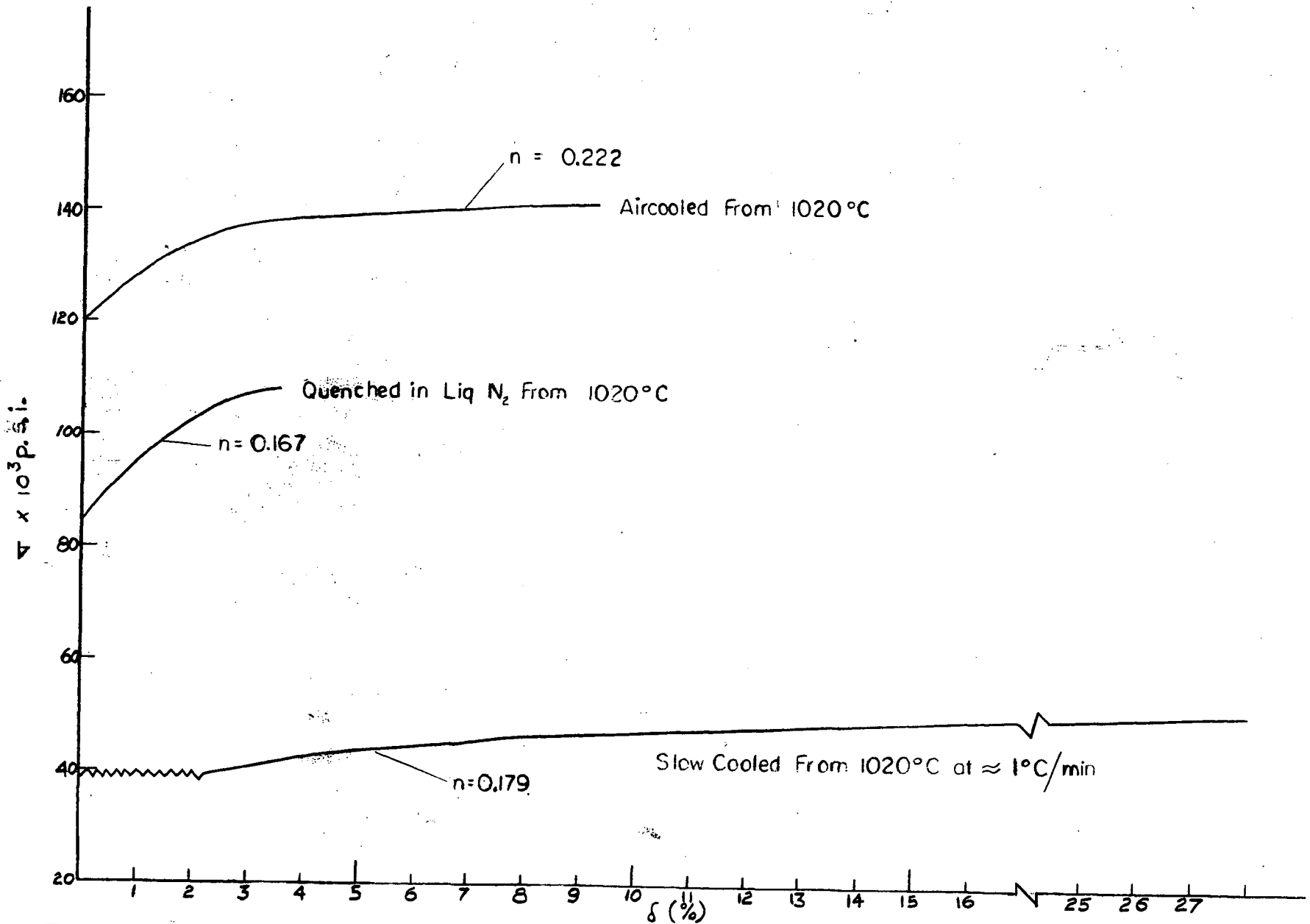


Figure 22 Stress Plastic Strain Curves For Representative Heat Treatments On-100+150 Mesh Powder Composites

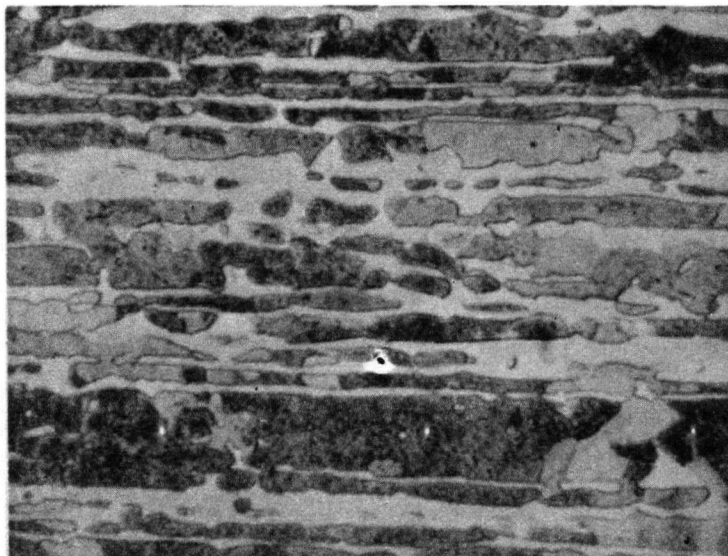


Figure 23. Photomicrograph of -325 mesh Powder Composite  
Quenched in liquid nitrogen and aged for 1 hour  
at  $-80^{\circ}\text{C}$ . Picric etch, X 1140.

(ii) Cooled at Rates of 1 to 25°C/second

Whereas the "aircooled" specimens were withdrawn a distance of 12 inches from the hot zone of the furnace in 4 seconds, for a cooling rate of 120 to 180°C/second, (Experimental Procedure, Section D.) tests were also made on specimens which were withdrawn from the furnace at slower rates to determine the effect of rate of cooling from the solution temperature.

- 30 seconds withdrawal time (estimated cooling rate 15 to 25°C/sec.)

Specimen Diameter	U.T.S. lbs/in <sup>2</sup>	Y.S. lbs/in <sup>2</sup>	Elong. %
0.035	122,800	113,700	15.5
0.035	116,300	110,100	14.3

- 14 minutes withdrawal time (estimated cooling rate 1/2 to 1°C/sec.)

Specimen Diameter	U.T.S. lbs/in <sup>2</sup>	Y.S. lbs/in <sup>2</sup>	Elong. %	Discontinuous Yield Elong. %
0.035	78,000	66,700	10.5	0.7
0.035	78,000	67,900	9.9	0.7

(iii) Furnace Cooled.

After solution treatment in a tube furnace, some specimens were left in the hot zone after the power to the furnace was cut off. The average rate of cooling was 500°C per hour for the first hour, and became increasingly slower as 30°C was approached.

Specimen Diameter	U.T.S. lbs/in <sup>2</sup>	Y.S. lbs/in <sup>2</sup>	Elong %	Discontinuous Yield Elong. %
0.035	64,500	52,600	28.3	3.5
0.035	64,500	52,000	26.6	2.8

(iv) Quenched in Liquid Nitrogen

Several solution treated specimens were quenched in liquid nitrogen from 1020°C, then brought to room temperature and tested within 5 minutes.

Specimen Diameter	U.T.S. lbs/in <sup>2</sup>	Y.S. lbs/in <sup>2</sup>	Elong. %
0.035	110,400	105,000	6.1
0.035	110,400	104,000	8.0

(v) Quenched in Liquid Nitrogen and Aged at -80°C.

Specimens were quenched to -196°C, then allowed to reheat and age at -80°C for various times as indicated below, (see also Figure 23).

Specimen Diameter	Ageing Time	U.T.S. lbs/in <sup>2</sup>	Y.S. lbs/in <sup>2</sup>	Elong. %
0.035	10 min.	118,700	111,800	11.2
0.035	30	111,000	105,000	10.5
0.035	1 hr.	117,000	110,200	10.7
0.035	3	114,700	106,800	11.7
0.035	6	111,200	106,500	7.9

(vi) Carburized at 920°C.

Specimens were "pack" carburized as outlined in Experimental Procedure for various times.

Specimen Diameter	Carburizing Time	U.T.S. lbs/in <sup>2</sup>	Y.S. lbs/in <sup>2</sup>	Elong. %
0.035	5 min.	125,900	119,500	16.9
0.035		118,000	109,700	10.2
0.035	20	118,800	105,000	7.0
0.035		126,300	109,200	6.8
0.035	100	109,800	73,800	1.6
0.035		110,100	72,200	1.3

The effect of long carburizing times on the microstructure is shown in Figure 24. It seems likely that the large pores are associated with the liberation of dissolved gas on cooling from the carburizing temperature.

Representative stress-plastic strain curves for the above mentioned heat treatments are shown in Figures 25 along with the corresponding work-hardening exponents. Figure 26 shows the variation of the yield stress of solution treated iron powders composites with cooling rate.

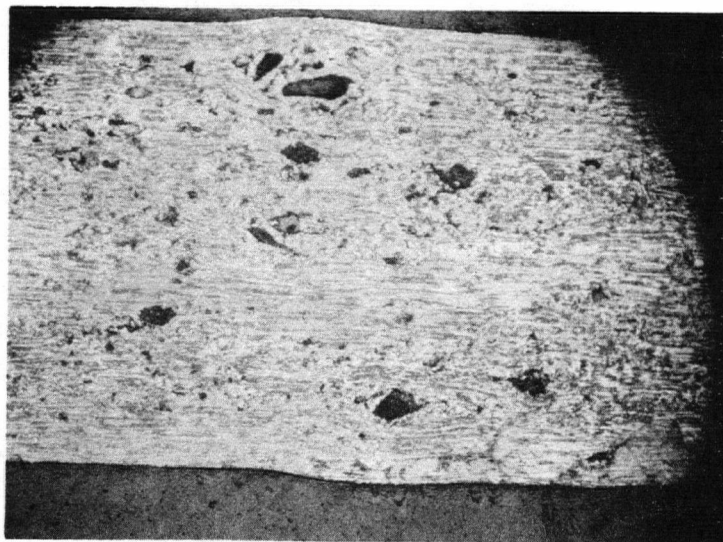


Figure 24. Photomicrograph of -325 mesh Powder Composite,  
Pack carburized at 920°C for 100 minutes, unetched.  
X 65.

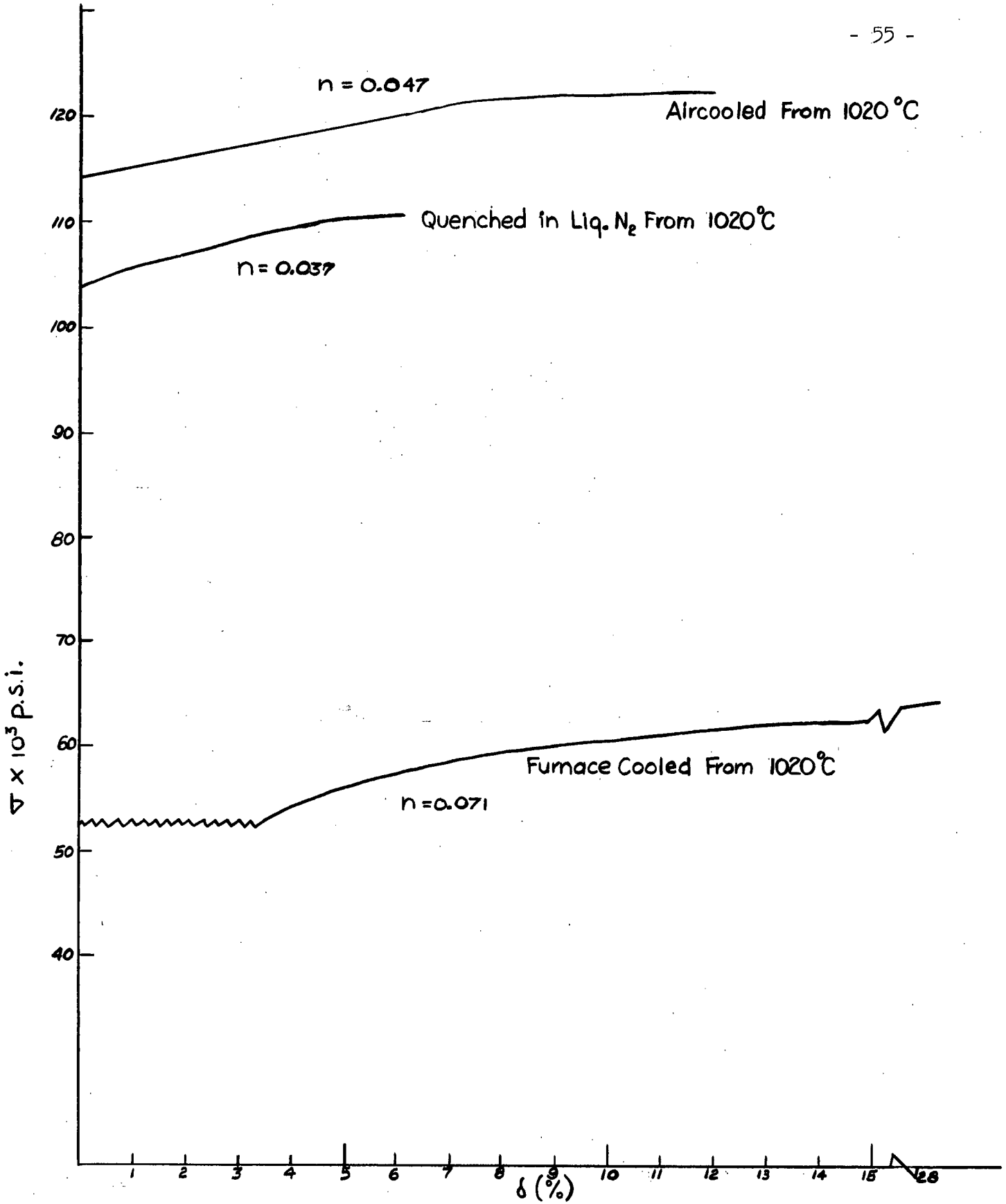


Figure 25 Stress-Plastic Strain Curves-Representative Heat Treatments On -325 Mesh Powder Composites

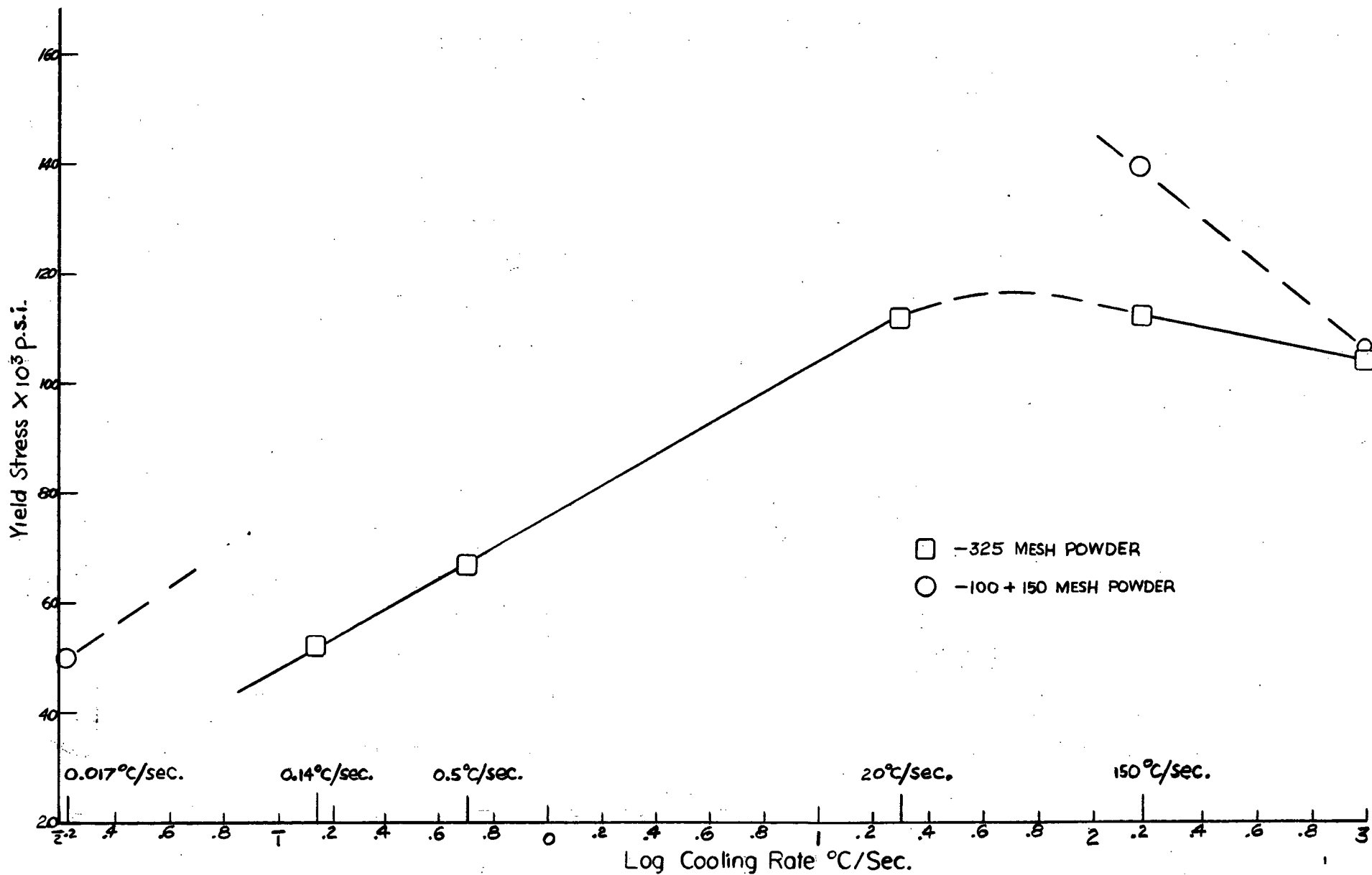


Figure 26 Y.S. Vs. Cooling Rate For Saturated Iron Powder Composites

#### IV. DISCUSSION

##### A. Structures and Aspect Ratios of Composites

Both methods used to produce a metal fibre reinforced composite proved to be suitable to some extent. For the purpose of fulfilling the objective of this work, however, the powder technique was superior. Much finer fibres could be produced and aspect ratios and interfibre spacings could be easily varied over a wide range. In addition, the material prepared from pure iron powders involved only two components, and was structurally simpler than that prepared from high carbon steel wire. That the fibres in specimens made from the coarser iron powder compacts did in fact have favourable aspect ratios can readily be proved. The diameters of the fibres are known as they were measured metallographically. However, as mentioned previously, the lengths of the fibres could not be obtained by metallographic examination. None the less, the volume of each iron particle is constant, and assuming that during the fabrication process the shape of the iron particle changes from a sphere to an ellipsoid of minor axis  $a=b$  and major axis  $c$ , then,

$$\text{Volume of fibre } V_f = \frac{4}{3} \pi abc = \frac{4}{3} \pi a^2 c = \frac{4}{3} \pi r^3$$

where  $r$  is the original iron sphere diameter. Therefore the aspect ratio of the fibres is  $\approx \frac{c}{a} = \frac{r^3}{a^3}$ . If the diameter of a specimen was reduced by a factor of 10 then "a" of the fibre =  $\frac{r}{10}$ , therefore  $\frac{c}{a} = 1000$ . (It should be noted that  $a$  is the maximum diameter of the fibre. The average diameter would be somewhat smaller.) Using this treatment, the aspect ratio of the fibres at a specimen diameter of 0.080 inches is, in theory, not less than 185:1. Substituting this value into the equation for the critical aspect ratio (equation 5) gives for the shear strength required

at the fibre-matrix interface

$$\tau = \frac{1}{185} \cdot \frac{1}{4} \sigma_f = \frac{\sigma_f}{740}$$

where  $\sigma_f$  is the tensile stress in the fibres. Thus, over the specimen size range investigated a maximum shear strength of  $\frac{\sigma_f}{740}$  is required in theory for full fibre reinforcement. The highest stress in an iron fibre encountered in this investigation is in the order of 240,000 psi. Consequently, the maximum shear stress required, even for a 0.080 inch diameter specimen is in the order of 325 psi. Since the shear yield stress for pure annealed polycrystalline copper is approximately 5,000 psi, the aspect ratios in all coarse iron powder composites in this investigation are believed to be favourable. The above analysis assumes that the fibres remain continuous during fabrication, which may not be true. However, the estimate of shear strength is conservatively high due to the nature of the other assumptions used.

Clearly the aspect ratios of fibres in saturated composites produced from -325 mesh iron powder were much less than discussed above (Figure 23). An estimate of the aspect ratio in this case is very difficult to make, since the coarser of the fibres present did retain a high ratio. Another feature of the finer powder composites is that a smaller volume fraction of iron was present ( 57%).

The aspect ratio in composites prepared from high carbon steel wires was approximately 200 in as-infiltrated specimens of normal test length (2 inches). With reduction of the infiltrated material by swaging and drawing the length of fibres in a test specimen cannot increase, and

the aspect ratio is then proportional to  $d_f^{-2}$  ( $d_f$  = fibre diameter). Thus a 90 per cent reduction in area of the composite produces at most a 90 per cent increase in the aspect ratio. Again, however, there is the possibility that the original wires do not remain continuous during reduction of the composite. Indeed, metallographic observations of as-drawn material indicate that some wire breakage did occur during fabrication. Thus it seems unlikely that the aspect ratio in wire composites was ever much greater than 200. At this ratio, the maximum shear strength required at the fibre matrix interface should not have exceeded 300 psi.

## B. Yielding Behaviour of Unsaturated Powder Composites

### 1. Heterogeneous Yielding

Heterogeneous yielding, involving relatively small load drops, was detected in some composites produced from iron powder. The occurrence of the phenomenon was not related to specimen size. In the case of saturated, heat-treated material, it only occurred in annealed specimens of low yield stress. There was no evidence to suggest that the discontinuous yielding was in any way due to breakage of individual fibres or to a loss of bonding at the fibre matrix interfaces. In fact, fibre breakage would cause serrations in the stress-strain curve at the ultimate stress (as observed by McDanel's et al. with copper-reinforced tungsten filaments<sup>8</sup>) and not at the yield stress. Thus, the heterogeneous yielding observed in powder composites is believed to be of the type normally observed in annealed iron and low-carbon steel, and to be attributable to the large volume fraction of iron (or the b.c.c. solution of copper in iron) which is present in these composites.

## 2. Size Dependence of Yield Stress

Figure 20 reveals that only a slight increase in yield stress occurred in unsaturated powder composites (from coarse powders) with decreasing specimen diameter over the size range investigated; i.e. corresponding to a range of individual fibre diameters of approximately 26 to 7 microns. There are several possible reasons for the increase observed.

a) There is a true size effect within the iron fibres over this size range, (a true size effect being one which is directly a function of the diameter such as the strength of a whisker.). There was no a priori reason, however, to expect such a size effect in a mixture of ductile phases, and it is unlikely that such an effect is involved.

b) The matrix mean free path decreases as the composite is reduced in diameter. Thus, strengthening of the matrix might be expected due to a reduction in the path length available for dislocation pile-up during initial plastic strain (i.e. a grain size effect exists).

c) As the composite is reduced in size, the dissolved copper content of the iron fibres increases with the accumulation of annealing time at 680°C. However, the maximum solubility of copper in iron at 680°C is reported to be 0.5 per cent. Moreover, although age-hardening is exhibited by alloys in this composition range, the solution hardening effect in this system is small.

It therefore seems probable that much of the 17.5 per cent increase in yield strength shown in Figure 20 is due to (b) with a contribution from (c).

## C. Yield Behaviour of Wire Composites

### 1. Origin of Two Yield Points

The load elongation curves for the wire composites exhibited two apparent yield points,  $Y_{P_{matrix}}$  and  $Y_{P_{composite}}$ . The corresponding "matrix yield stress" increased fairly rapidly with decreasing specimen diameter (Figure 12). Coupling this with the observations shown in Figure 13, in which the thickness of the copper coating on the outside of the specimen is related to specimen diameter, suggests that the initial yielding observed was due to a grip effect. It is suggested that the copper coating yielded in the grips giving rise to  $Y_{P_{matrix}}$ . As evidence of this, at smaller specimen diameters corresponding to thinner copper coatings, the matrix yield stress rose, probably due to increasing restraint from the steel fibres. In fact, at small specimen diameters the matrix yield stress became very close in value to that which has been termed the composite yield stress. Consequently, it is believed that only the latter yield stress is truly indicative of the properties of the composites.

### 2. Heterogeneous Yielding

The extent of heterogeneous yielding in wire composites was distinctly related to composite diameter (Figure 14). The phenomenon was also much more marked in wire than in powder composites. Since discontinuous yielding was only observed in materials of relatively low composite yield stress, it is unlikely that it can be attributed even partially to a grip effect; i.e. irregular grip slippage. Also, breakage of fibres would be expected to cause serrations to appear in the stress strain curve at higher stresses <sup>8</sup> rather than just at the onset of yielding.

It was demonstrated that a single, spheroidize-annealed, steel wire exhibited discontinuous yielding of the type observed in mild steel. It has been stated elsewhere<sup>23</sup> that a spheroidized eutectoid in a high carbon steel can exhibit the phenomenon, whereas a pearlitic structure of the same overall composition does not. Bredz and Schwartzbart<sup>24</sup> have observed a decarburizing phenomenon when copper was melted in contact with steels of various carbon contents. The carbon (due to the influence of the copper) became concentrated at the grain boundaries of the steel.

The 0.012 inches diameter steel wires contained in the composites used in this investigation were in contact with liquid copper at 2100°F for 10 minutes followed by quenching. Iron at this temperature can contain up to 8.5 per cent copper in solution. It has been stated elsewhere<sup>17</sup> that a -100 +150 mesh pure iron powder composite becomes saturated with copper in approximately 200 minutes of infiltration time at 1100°C. Thus, due to the large size of the individual wires and relatively short time in contact with liquid copper, it is felt that only the surface of the wires was initially saturated with copper. The structure of the steel fibres then, prior to the initial swaging operation, was tempered martensite (quenching from 1150°C followed by tempering at 680°C).

Experiments involving the effect of cold work and strain annealing indicated that heterogeneous yielding in the wire composites might be of the normal mild steel type observed in spheroidized high-carbon steels. However, the size dependence of the phenomenon is not adequately explained on this basis. Moreover, the fact that a marked decrease in wire composite yield strength occurred at sizes where heterogeneous yielding was a maximum suggests that another mechanism may be involved in the process.

It is proposed that much of the discontinuous yielding in wire composites is attributable to shearing at the matrix-fibre interfaces. With progressive reduction and annealing of the composite, carbon segregates to the steel wire surfaces (as per Bredz and Schwartzbart<sup>24</sup>) and eventually appears as graphite at the interface. The fact that this phenomenon would be dependent on total annealing time and hence specimen diameter accounts for the observed variation in extent of the discontinuous yielding with specimen size shown in Figure 14. Thus, with decreasing composite diameter, down to about 0.046 inches, the fraction of total interface area on which shearing can occur is increasing. Below this size, separation over all the matrix fibre interfaces occurs after progressively less total strain. This argument predicts that below 0.046 inches diameter, the tensile load on the composites is being carried entirely by the matrix in the early stages of flow. The strain-hardening behaviour (Table II, page 32) does not support this model too well, however.

The observed effects of ageing and cold work can be rationalized in terms of the proposed interface-shear mechanism. At the specimen diameter which exhibited the maximum amount of discontinuous yielding, i.e. 0.046 inches, cold working of the specimen to a reduction of 4 1/2 per cent not only eliminated the discontinuous yielding but also raised the yield stress to 44,000 psi which is an increase of approximately 33 per cent over the annealed condition (Figure 9). This implies that cold working has partially restored the bond between the fibres and the matrix, by mechanically breaking down graphite or other interfering layers. Ageing of specimens in this size range for 1 hour at 200°C partially restored the discontinuous yielding

while also slightly raising the composite yield stress (by approximately 6 per cent). According to the interface-shear argument above, this would imply that the ageing treatment has allowed the creation of new shear points or areas which shear at higher stress values than in the initial specimen.

Optical microscopy, unfortunately, failed to reveal clearly the formation of the weakening interface layers postulated above. Also, there was no positive evidence in the microstructure of partially deformed or fractured wire composites that the shear mechanism had or had not been operative. The main basis for the postulation that interfacial shear must have occurred in these materials was the observed dependence of composite yield stress on specimen size, as discussed in the following section.

### 3. Size Dependence of Yield Stress

The composite yield stress versus specimen diameter curve for the steel wire composites (Figure 9) shows a distinct anomaly within a critical size range.

The composites used in this investigation were given one hour anneals at 680°C subsequent to each 40 per cent reduction in cross-sectional area. This annealing tended to further spheroidize and coarsen the carbide in the steel wires (Figure 6). Associated with spheroidization would be expected a slight lowering of the yield strength of the fibres with decreasing fibre diameter (increasing total annealing time). The matrix, on the other hand, would be expected to show an increase in strength with decreasing specimen diameter due to a matrix mean free path effect analogous to the major strengthening mechanism proposed for the iron powder composites.

Based on observations reported for other systems, yield stress increases with  $\lambda^{-1/2}$  where  $\lambda$  = mean free path.

The fibre strength curve, it is suggested, is interrupted by shearing at the matrix-fibre interface. The matrix carries the entire load on the composite once shearing of the interface is complete. However, relatively high stresses (approaching the true fracture stress of the matrix alloy) can be carried since necking of the matrix is restrained by the fibres, i.e. there is a hydrostatic pressure effect in the matrix. Superimposing the above effects gives the schematic summation curve shown in Figure 27, which is of the general form of the experimental yield stress curve obtained for wire composites (Figure 9).

#### D. Effect of Heat Treatment on Saturated Powder Composites

The strengths observed in powder composites after saturating the iron fibres with copper at 1020°C were extremely dependent on cooling rate from 1020°C. Consideration of the possible phase transformations involved became necessary in order to explain this behaviour and to explain the relatively high strengths obtainable in saturated composites.

The solubility of copper in  $\alpha$ -iron at 1020°C has been reported at 7-8 per cent by weight. Krantz<sup>17</sup> has shown that saturation of -100 +150 mesh particles of iron with copper will occur at 1100°C in approximately 200 minutes. Thus, powder composites which were solution treated in the present studies as described previously, involved copper-saturated iron fibres.

Previous reported studies of non-equilibrium phase transformations in the iron-copper system have been largely confined to alloys containing up to 4 weight per cent copper. It is recognized that these alloys can be

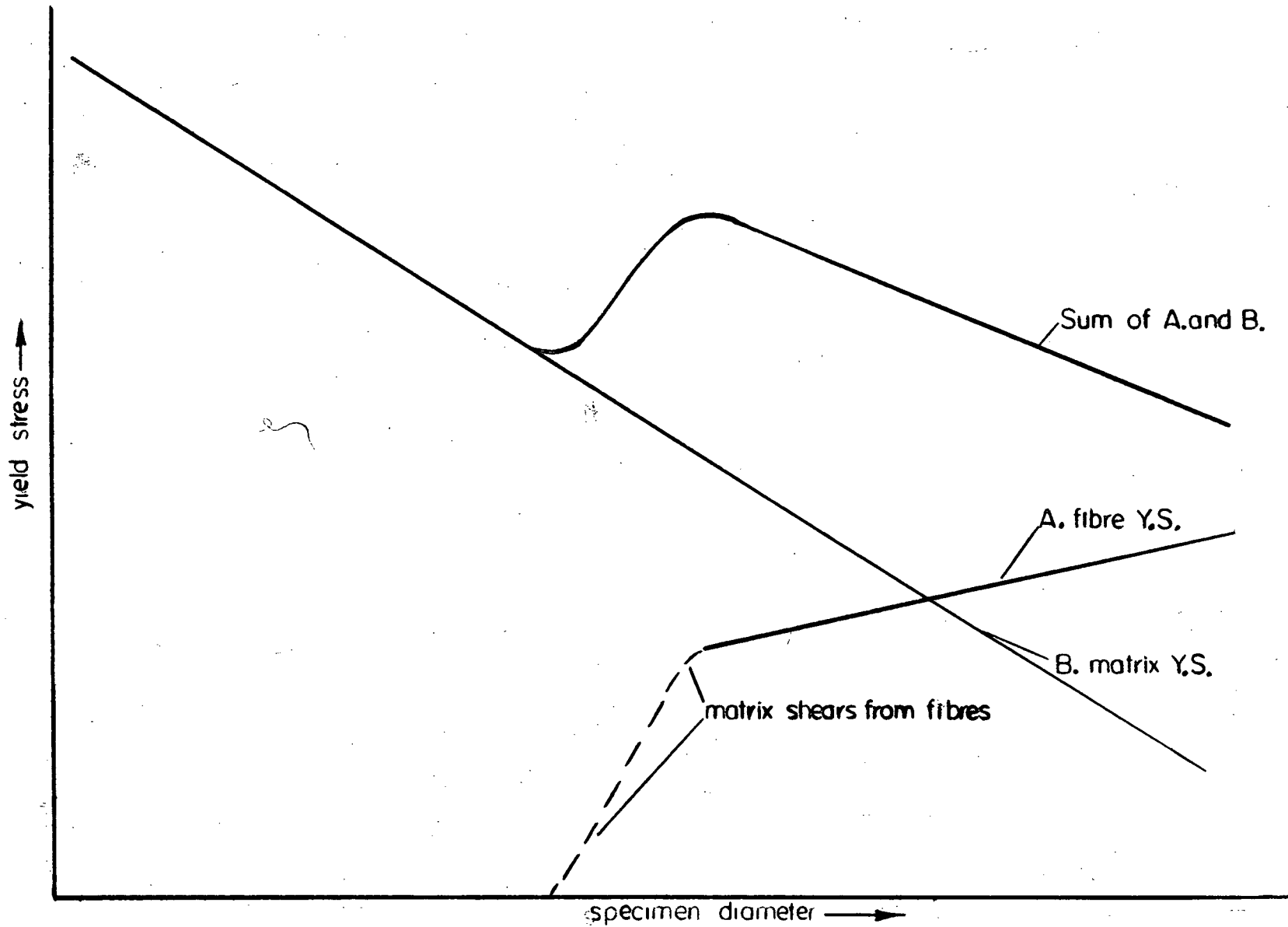


Figure 27 Specimen Diameter Vs. Predicted Matrix and Fibre Strengths

solution treated and quenched from above or below the eutectoid temperature, then precipitation-hardened at a few hundred degrees Centigrade<sup>20</sup>. However, no studies have been reported in the literature of the non-equilibrium decomposition of the eutectoid at 4 weight per cent copper. Specifically, there is no reference to a martensite transformation in this system in the extensive studies of such transformations by Zackay et al<sup>26</sup> or Bilby and Christian<sup>28</sup>.

White<sup>25</sup> performed some unpublished work on iron - 6 weight per cent copper alloys prepared by melting and casting. He hot and cold rolled ingots to obtain strip material which was cut into shaped tensile specimens. These were homogenized (solution treated) at 1100°C, cooled at various rates to 20°C, and tested in tension with the following results:

1. Water Quenched From 1100°C

U.T.S. lbs/in <sup>2</sup>	Y.S. lbs/in <sup>2</sup>	Elong. %	Hardness Rockwell
109,000	n.a.	6.0	C 5
107,000	1100,000	6.0	B 90

2. "Aircooled" From 1100°C

U.T.S. lbs/in <sup>2</sup>	Y.S. lbs/in <sup>2</sup>	Elong. %	Hardness Rockwell
153,000	143,000	4.0	C 31
151,000	141,000	4.0	C 31
156,000	146,000	5.0	C 32

3. Furnace Cooled From 1100°C

U.T.S. lbs/in <sup>2</sup>	Y.S. lbs/in <sup>2</sup>	Elong %	Hardness Rockwell
72,000	61,600	15	B 66
76,700	64,800	16	B 67
72,500	61,600	18	B 65

White also examined the effect of reheating aircooled specimens for 1 hour at various temperatures, followed by aircooling to 20°C.

4. "Aircooled" From 1100°C, Reheated to 400°C for 1 hour.

U.T.S. lbs/in <sup>2</sup>	Y.S. lbs/in <sup>2</sup>	Elong %
130,000	119,000	10
127,000	117,000	10
135,000	123,000	7

5. "Aircooled" From 1100°C, Reheated to 600°C for 1 hour.

U.T.S. lbs/in <sup>2</sup>	Y.S. lbs/in <sup>2</sup>	Elong %
89,000	80,000	13
91,000	84,000	13
95,000	86,000	13

6. "Aircooled" From 1100°C, Reheated to 750°C for 1 hour.

U.T.S. lbs/in <sup>2</sup>	Y.S. lbs/in <sup>2</sup>	Elong %
84,000	74,000	16
85,000	79,000	16
80,000	72,000	15

These results bear a clear relationship to those obtained in the present studies by heat-treating powder composites. In view of the known

and rather small effects of age-hardening the  $\alpha$  solid solution in Fe-Cu, the enormous difference between the air-cooled and furnace-cooled 6-8% Cu alloys cannot be explained in such terms. In fact, consistent with the phase diagram for Fe-Cu, it is difficult to explain the high strength of aircooled (or even quenched) materials by other than a martensite transformation. It remains to explain why the properties of these alloys respond to cooling rate in the manner observed.

There are several known martensite transformations including Cu-Al<sup>26</sup> and Fe-Ni<sup>27</sup> in which the  $M_s$  and  $M_f$  temperatures are strongly dependent on slight variations in the concentrations of the minor components. Of particular interest is the Cu-Al system where a change in Al concentration of from 11 to 15% (hypereutectoid range) lowers the  $M_s$  by approximately  $450^\circ\text{C}$ <sup>26</sup>. It is felt that a similar effect occurs in the Fe-Cu system, with increasing copper contents lowering the  $M_s$ .

For purposes of discussion, consider the quenching of a homogeneous Fe-7% Cu alloy from  $1020^\circ\text{C}$ . Quenching at a rate greater than some certain critical value would allow virtually full retention of the copper in solution. The high copper concentration, however, will depress the value of the  $M_s$  and  $M_f$  from those which would exist at a lower copper concentration. Thus, the amount of martensite that would be formed at a particular temperature between  $M_s$  and  $M_f$  for the 7% copper alloy would be less than that resulting from quenching to the same temperature an alloy of lower copper concentration. Compare this result with that predicted from cooling the same alloy at a lower rate (i.e. below the critical rate).

This would allow partial precipitation of the epsilon phase during cooling. In this manner, the copper content that would be retained in solid solution on further cooling would be somewhat reduced and the residual  $\gamma$  would have a higher  $M_s$  and  $M_f$ . The net consequence is that a substantially greater amount of martensite would result on further cooling to the reference temperature, provided the rate of cooling was rapid enough in this range of temperature.

Figure 28 shows a suggested cooling-transformation diagram for the iron-7% copper alloy, the form of which is consistent with the above argument, and the use of which permits observations in the present investigation to be explained.

It is interesting to note that in the Cu-Al system martensite transformations are reported only for hypereutectoid compositions<sup>28</sup>. If similar behaviour is exhibited by the Fe-Cu system, this could explain the absence of previous observations of a martensite reaction, since nearly all earlier work with this system has been with alloys of less than 4 weight per cent copper.

Some of the saturated powder composites studied in the present work were quenched in liquid nitrogen from the solution treatment temperature and then tested in tension at room temperature. For the above mechanism to explain the results obtained, the martensite transformation would be required to be completely reversible, a condition that exists in most other systems which exhibit martensitic type transformations<sup>29</sup>.

In the powder composites the rate of cooling due to "aircooling" is apparently such as to produce the maximum amount of martensitic phase consistent with the proposed transformation. Reheating of "aircooled"

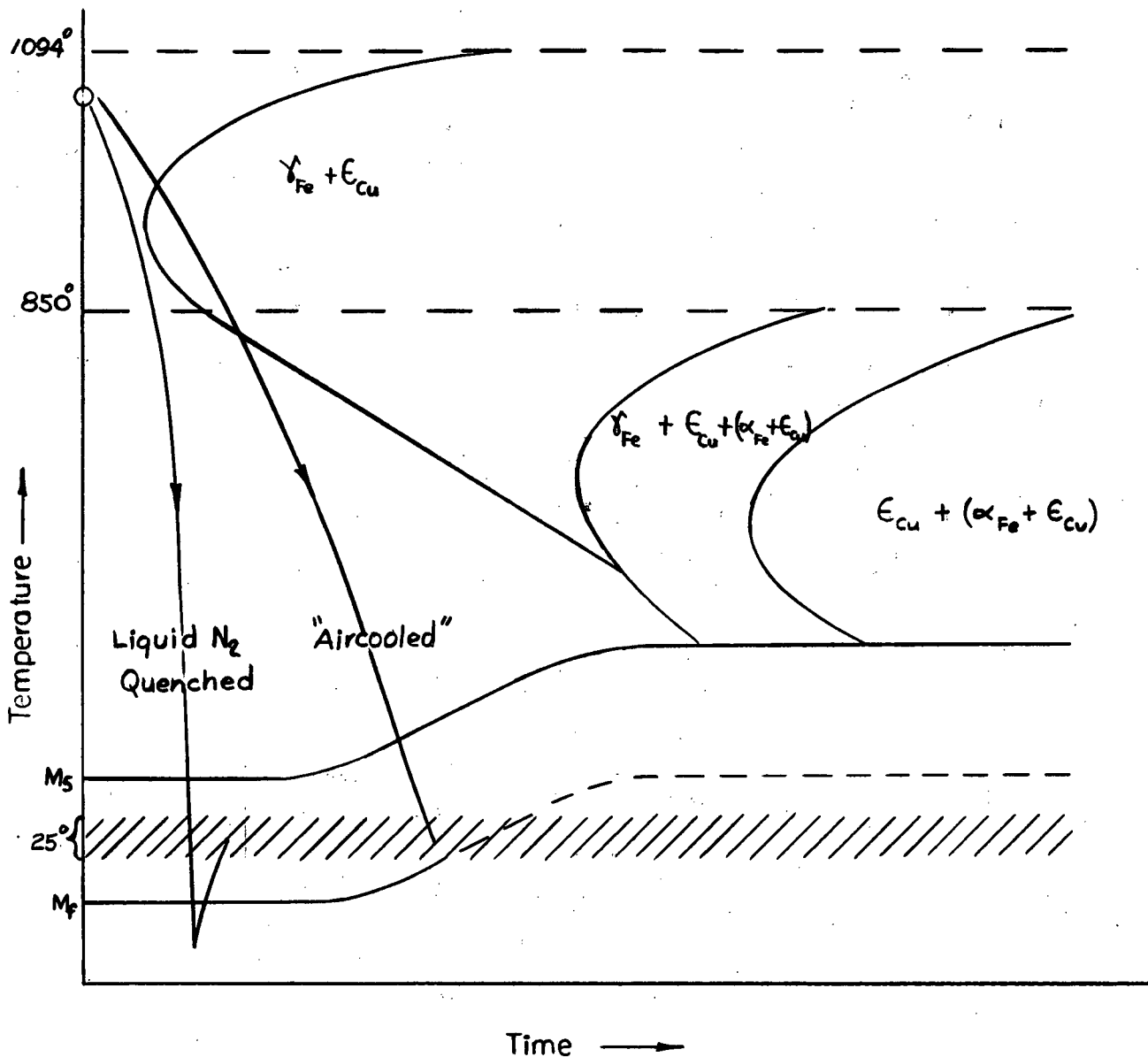


Figure 28 Cooling Rate-Transformation Diagram For an Iron - 7% Copper Alloy

specimens at 400°C for one hour is presumed to have partially tempered the martensite, whereas a one hour treatment at 750°C has apparently transformed the metastable martensitic phase into a relatively coarse mixture of low-copper  $\alpha$  and the epsilon phase. The latter transformation would be expected to allow a return of heterogeneous yielding in the ferrite, a condition which was, in fact, observed.

An interesting result of the heat treatments of "saturated" composites (and one which cannot be explained in terms of a simple martensitic transformation) is the apparent age-hardening of specimens quenched in liquid nitrogen and held at room temperature. In studies of precipitation of  $\epsilon$  from  $\alpha$  it has been revealed that maximum hardness occurs as a result of ageing at temperatures between 400 and 700°C.<sup>20</sup> In addition, measureable precipitation of  $\alpha$  from  $\epsilon$  occurs only at temperatures above 600°C and then only to a very limited extent<sup>19</sup>. Thus it is apparent that the normal precipitation phenomenon generally observed in the Fe-Cu system does not apply in this case.

It is possible that some tempering of the high copper martensite formed by quenching the saturated (7-8% copper)  $\gamma$  occurs at 20°C in view of the high degree of supersaturation involved. Also, precipitation from retained  $\gamma$  may occur. This could in turn cause hardening of the existing martensite by the formation of coherency strains, and/or result in the conversion of some retained  $\gamma$  to lower-copper martensite.

Of particular interest is Figure 26, which shows the variation of the yield stress of the composites with changes in cooling rate from the saturation temperature. It is apparent that the maximum strengths in the composites occur as a result of cooling rates of between 20 and 150°C/sec.

The curve also shows virtually a linear dependence of yield stress with variations in cooling rates less than the values just mentioned. This is consistent with what would be expected from a consideration of the cooling-temperature curve shown in Figure 28. Slower cooling rates would allow diffusion-controlled phase transformations to occur during cooling with a subsequent softening effect.

#### E. Deformation Behaviour of Metal Fibre Reinforced Metals

Krantz<sup>17</sup> has examined the properties in the bulk form of a copper-iron alloy essentially identical to the matrix alloy in these fibre composites. He found the ultimate tensile strength to be 47,000 psi with an elongation to fracture of 30 per cent in 1 inch. The true fracture stress however, can be taken as approximately 118,000 psi on the basis of area at the fracture.

The saturated and heat-treated powder composites provided an excellent opportunity to examine the effect of the relative strengths of fibre and matrix on composite properties. Thus in furnace-cooled material, the yield and ultimate strengths were low (39,000 and 50,000 psi respectively) and the elongation to fracture was high (27 per cent). These properties are in fact similar to those of unsaturated composites of similar size. Clearly in this case, deformation of the matrix is not being restricted appreciably by the fibres, since the latter are ferrite ( $\alpha$ ) of low dissolved copper content with deformation behaviour similar to that of the matrix.

By contrast, aircooled composites contained fibres for which the yield and ultimate strengths could be expected to be at least 142,000 and 152,000 psi respectively according to White's results. The fact that such composites exhibited strengths of 110,000 psi (yield) and 140,000 psi

(ultimate) can be accounted for by a "size effect" in the matrix rather than in the fibres. The high-strength fibres constitute strong barriers to flow in the matrix. That is, dislocation pile-up in the very early stages of plastic strain in the matrix (prior to the attainment of the reported yield stress) leads to very rapid matrix hardening. The fact that the length of pile-ups is severely restricted at the small composite and fibre diameters involved, means that the "matrix size effect" being realised is large. The matrix accordingly can support stresses much higher than its bulk ultimate strength, perhaps approaching its true fracture stress.

Similar arguments provide an explanation for the strength properties of composites with other thermal histories in the present work. It remains, however, to compare the theories advanced by previous investigators with the arguments proposed above.

The "fibre size effect" reported by Jech et al.<sup>5</sup> in tungsten fibre-reinforced copper can probably be partly attributed to the matrix size effect discussed previously.

On the basis of several assumptions, an expression for the predicted variation of composite strength with matrix mean free path can be developed mathematically.

Assuming that the fibres in the composite are continuous and have the uniformly packed array shown in Figure 29, then the area of a fibre can be related to the total composite area as follows:

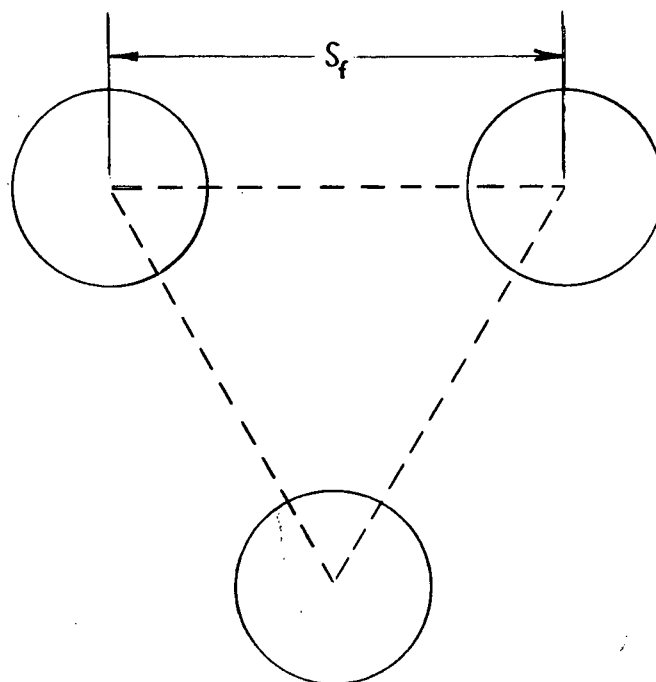


Figure 29. Assumed Fibre Distribution

Total area of triangle in Figure 29

$$A_t = \frac{1}{2} S_f \frac{\sqrt{3}}{2} S_f = \frac{\sqrt{3}}{4} S_f^2$$

Area of fibre inside triangle

$$A_f = \frac{1}{2} d_f^2 \frac{\pi}{4} = \frac{\pi}{8} d_f^2$$

$$\frac{A_f}{A_t} = \frac{\pi d_f^2}{2\sqrt{3} S_f^2} = \text{Volume Fraction Fibres} = N_f$$

Thus, the interfibre spacing ( $S_f$ ) is:

$$S_f = \sqrt{\frac{\pi d_f^2}{2 \cdot 3 N_f}}$$

Also, since there is a linear relationship between interfibre spacing and matrix mean free path for the case of continuous fibres, then:

$$\text{M.F.P.} \propto \frac{d_f}{\sqrt{N_f}}$$

Gensamer, working with steels, has shown that the strength of a matrix containing a hard dispersed phase is proportional to the log of reciprocal mean free path. Other investigators, with various two-phase systems have found a (M.F.P.)<sup>-1/2</sup> dependence of strength. Mathematically, both these functions are quite similar. Therefore, assuming a (M.F.P.)<sup>-1/2</sup> relationship,

$$\text{strength of matrix } (\sigma_m) \propto (\text{M.F.P.})^{-1/2} \propto \frac{N_f^{0.25}}{\sqrt{d_f}} \dots (7)$$

It now becomes necessary to modify the theory of combined action, which assumes that the matrix strength  $\sigma_m$  is independent of the volume

fraction or diameter of the fibres present, i.e.

$$\sigma_c = A_f \sigma_f + A_m \sigma_m$$

Consider the effect of increasing the volume fraction of the fibres (i.e.  $A_f$ ) while keeping  $d_f$  constant. This will decrease the value of  $A_m$ , the volume fraction of the matrix. The theory of combined action indicates that the composite strength increase is linear, i.e. there is no accompanying change in the values of the fibre and matrix stresses. The theory proposed however, is that the matrix strength is proportional to (volume fraction of fibres)<sup>0.25</sup> and thus any increase in the volume fraction of fibres causes an increase in the strength of the matrix. The effect, although relatively small, has maximum influence at low volume fractions of fibres (i.e. less than 20%). This could possibly account for the discrepancy between the experimental points and the calculated straight line observed by McDanel's et al.<sup>8</sup> In their work, plots of composite ultimate tensile stress versus volume per cent fibres for three separate fibre diameters gave experimental values at low volume per cent fibres that were greater than the values calculated from the theory of combined action.

Equation (7) indicates an inverse square root dependence of matrix strength with fibre diameter. The effect is greater, the smaller the diameter of the fibre. Unfortunately, there is no direct experimental evidence to support this premise.

It is thus proposed that the existing theory for predicting the strength of fibre-reinforced composites should be modified to become:

$$\sigma_c = A_f \sigma_f + A_m \sigma_m + A_f^{1/4} K d_f^{-1/2} \dots (8)$$

where K is a constant depending on the relative strengths of the fibre and the matrix.

A value of K can be calculated from one set of results obtained in this investigation, namely, the "aircooling" of the coarse iron powder composites. Substituting pertinent values into equation (8) and solving gives K equal to 281 lbs/in<sup>3/2</sup> at a fibre diameter of 10 microns. If K depends only on the relative strengths of the fibre and the matrix then equation (8) should give the composite strength for the "aircooled" -325 mesh powder composites with a substitution of the corresponding values of  $A_f$ ,  $A_m$  and  $d_f$ . Such a calculation gives a value for the composite strength of 137,600 psi which is 13 per cent greater than that determined experimentally (122,000 psi). The theory of combined action, on the other hand, predicts 109,500 psi as the composite strength.

The calculated value of the strength is based on the assumption that the mean free path is linearly dependent on the diameter of the fibre (i.e. continuous fibres are assumed). This is not true for the case of -325 mesh powder composites (Figure 23). Apparently the mean free path is several times greater than has been assumed in the mathematical development. This will have the effect of lowering the value of the third term in equation (8), thus bringing the calculated value closer to that determined experimentally. On the other hand, it is hard to visualize any additional effect increasing the strength as calculated from the theory of combined action, (apart from increasing the strength of the fibres due to a "size effect", a condition which has not been found to occur in this investigation).

## V. CONCLUSIONS

1. No strengthening effect has been observed in fibre-reinforced composites in this work which can be attributed to fibre "size effects". However, the strength of metal fibre reinforced metal composites is believed to be greatly influenced by a "size effect" in the matrix.

2. Any factor which affects the matrix mean free path (e.g. volume fraction of fibre and fibre diameter) can be expected to affect composite strength. However, the extent to which such effects are important is controlled by the relative hardness or strength of the fibre; i.e. by its effectiveness as a barrier to flow in the matrix.

3. The following modification of the theory of combined action is proposed for predicting the strength of a fibre-reinforced composite:

$$\sigma_c = A_f \sigma_f + A_m \sigma_m + A_f^{+1/4} K d_f^{-1/2}$$

where A is volume fraction, f refers to fibre, m refers to matrix,  $d_f$  is fibre diameter and K is a constant whose value depends on the hardness of the fibre.

4. In composites of copper reinforced by steel wires, weakening of the matrix-fibre interface can occur as a consequence of carbon segregation to the interface. This leads to shearing at the interface in the early stages of tensile deformation.

5. Alloys containing 6 to 8 weight per cent copper in iron exhibit a martensite transformation when cooled from the  $\gamma$  region of the Fe-Cu phase diagram. The martensite formed at 6 per cent copper has an ultimate strength of approximately 150,000 psi and exhibits appreciable ductility. This martensite transformation apparently has not been observed heretofore in studies by other investigators of Fe-Cu alloys.

## VI. SUGGESTED FUTURE WORK

This work has been primarily of an exploratory nature and the results have suggested directions of future work which might be profitably explored.

It is recommended that further studies be carried out on the phase transformations in hypereutectoid Fe-Cu alloys of bulk form.

Experimental verification of the proposed rule for predicting composite strength is recommended. This could be done by the extension of experimental work to other systems and by means of experiments in which the fibre size,  $d_f$ , is varied without varying the inherent fibre strength.

In addition, it is felt that this work could be extended to even smaller fibre sizes and/or smaller matrix mean free path distances by a judicious choice of wire drawing equipment, powder sizes, and heat treating conditions. Saturation of the fibres with copper prior to final drawing could help to obtain the desired result.

VII. BIBLIOGRAPHY

1. Coleman, B.D., J. Mech and Phys. of Solids, 7, 60 (1958).
2. Parratt, N. J., Rubber and Plastic Age, 41 (3), 263 (1960).
3. Dietz, A. G. H., "Design Theory of Reinforced Plastics", Fiberglass Reinforced Plastics, Chapter 9, Reinhold, New York, N.Y., (1954).
4. Sutton, W. H., J. Amer. Rocket Society, April 1962, 593.
5. Jech, R. W., McDanel, D. L., and Weeton, J. W., "Composite Materials and Composite Structures", Proc. Sixth Sagamore Ordnance Materials Conference, August 1959, 116.
6. Kelly, A., Private communication.
7. Cratchley, D., Powder Met., (11), 59 (1963).
8. McDanel, D. L., Jech, R. W., Weeton, J. W., Technical Note D-1881, N.A.S.A., Washington D.C., October 1963.
9. Dow, N.F., Technical Information Series, R 63SD61, General Electric, Space Sciences Laboratory, (1961).
10. Koppenaal, A., Parikh, N., Trans. A.I.M.E., 224, 1173 (1963).
11. Sutton, W. H., Rep. No. R 62SD65 Class 1, General Electric, (1962).
12. Whitehurst, H. B., Michener, J. W., Lockwood, P., Proc. Sixth Sagamore Ordnance Materials Conference, August 1959, 248.
13. Cratchley, D., Heywood, D. M., to be published.
14. Wagner, H. J., Battelle Technical Review, 12 (12) 8 (1963).
15. Sutton, W. H., Chorner, J., Metals Engineering Quarterly, 3 (1), 1963.
16. Roberts, D. A., Memorandum 80, Defence Metals Information Center, January 1961.
17. Krantz, T., Private communication based on M.A.Sc. project, University of British Columbia.
18. Wriedt, H. A., Darken, L. S., Trans. A.I.M.E. 218, (1960).
19. Newkirk, J. B., Trans. A.I.M.E. 209, 1214 (1957).
20. Hornbogen, E., Glenn, R.C., Trans. A.I.M.E., 218, 1064 (1960).

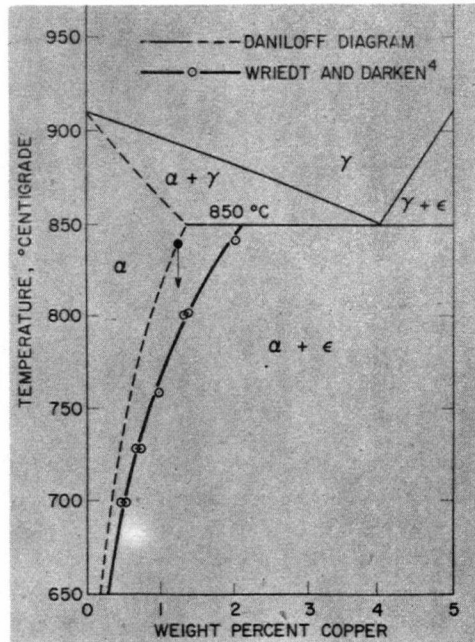
Bibliography Continued...

21. Bandi, A., Chem. Rev. 52, 417 (1953).
22. Snowball, R.F., M.A.Sc. Thesis, University of British Columbia, 1961.
23. Gensamer, M., Pearsall, E.B., Pellini, W.S., Low Jr., J.R., Trans. A.S.M. 30, 983 (1942).
24. Brédz, N., Schwartzbart, H., Welding Research Supp. 41, 129-S (1962).
25. White, H., Unpublished work, University of British Columbia, 1963.
26. Zackay, V.F., Justusson, M.W., Schmatz, D.J., "Strengthening Mechanisms in Solids", Strengthening by Martensitic Transformations, Chapter 7, A.S.M. (1960).
27. Kaufman, L. Cohen, M., "The Mechanism of Phase Transformations in Metals", Nucleation in Martensitic Transformations, Institute of Metals, London, (1956) 187.
28. Bilby, B.A., Christian, J.W., Ibid. 121.
29. Troiano, A.R., Greninger, A.B., A.S.M. Handbook (1948) 263.

VIII. APPENDICES

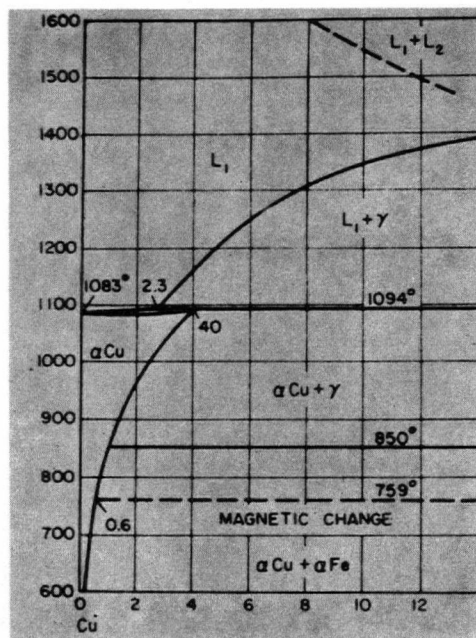
APPENDIX I.

Iron-Copper System



Fe-rich End

Reproduced from Wriedt and Darken, Trans. A.I.M.E., 218, (1960)



Cu-rich End

Reproduced from Butts, "Copper, the Metal, Its Alloys and Compounds",  
New York, 471 (1954).

## APPENDIX II.

A. Data for Steel Wire-Reinforced Composites

Composite Number	Specimen Diameter (in)	Y.S. Matrix psi	Y.S. Composite psi	U.T.S. psi	Disc. Yield Unit Strain (in)
W-1-A	0.098	5,800	21,600	47,200	0
	0.089	8,600	26,500	48,700	0
	0.075	10,500	31,300	68,500	0
	0.067	18,200	35,100	63,100	0.023
	0.052	21,500	34,300	54,400	0.040
	0.051	26,100	32,000	53,700	0.036
	0.047	16,800	38,300	53,400	0.063
	0.047	23,600	39,200	54,700	0.063
	0.043	18,200	34,000	61,700	0.047
	0.038	19,500	36,300	64,500	0.034
0.034	24,000	45,400	74,500	0.028	
W-2-A	0.057	15,000	42,700	49,600	0.046
	0.047	18,700	33,800	42,800	0.050
	0.047	16,800	31,900	37,800	n.a.
	0.047	15,900	34,500	42,600	0.043
W-3-A	0.070	14,500	34,400	63,400	0.039
	0.063	12,300	39,200	68,600	0.035
	0.060	13,900	41,300	66,400	0.030
	0.058	18,300	38,600	56,100	0.038
	0.053	15,200	35,300	52,500	0.035
	0.051	14,000	32,000	48,100	0.046
	0.042	21,400	33,000	46,400	0.017
	0.040	25,500	33,500	40,000	0.030
	0.036	24,500	36,300	44,200	0.027
	0.036	31,400	35,400	54,800	0.018
	0.032	40,000	44,100	74,700	0.000
	0.022	45,200	50,800	71,200	0.020

## Appendix II. Continued..

B. Data for Iron Powder Composites

Composite Number	Specimen Diameter (in)	Composite Yield Stress psi	U.T.S. psi	Disc. Yield Elong. (%)
Powder 2	0.096	29,700	41,100	0
	0.076	28,500	45,600	0
	0.073	37,200	45,700	0.1
	0.061	29,400	40,000	*
	0.057	33,600	42,200	*
	0.046	29,100	44,800	*
	0.030	33,000	49,400	4.2
	0.027	33,500	48,800	4.1
Powder 3	0.077	33,100	46,800	2.1
	0.074	32,900	43,800	0
	0.071	28,700	42,400	*
	0.069	29,800	42,600	1.4
	0.063	27,900	45,400	1.8
	0.059	26,200	43,500	0.8
	0.051	34,000	39,900	2.9
	0.046	30,600	43,500	1.0
	0.040	38,000	47,500	3.2
	0.038	33,200	41,800	3.0
	0.034	33,000	45,600	2.5
	0.028	34,700	42,300	*
	0.025	34,700	41,600	*

\* Discontinuous Yielding was present but range over which it acted could not be clearly defined.